# Assessment of High Purity Mesenchymal Stromal Cells Derived Extracellular Vesicles Presenting NRP1 Show Functional Suppression of Activated Immune Cells

A Thesis Submitted to the Faculty of Medicine of the University of Ottawa

In Partial Fulfillment of the Requirements for the Degree of Master of Science in Biochemistry

By Jonathan Gobin

Supervisors: Dr. Lisheng Wang, Dr. Michael Rosu-Myles

University of Ottawa

Ottawa, Ontario, Canada

Faculty of Medicine

Department of Biochemistry, Microbiology, and Immunology

Contributions:

All the experiments in this study were designed and analyzed by myself.

- hBM-MSC Expansion, Hollow Fibre Bioreactor Culture and, Proteomics sample isolation - performed by Gauri Muradia (Research Technician; Lab Member)
- hBM-MSC Differentiation and MSC Immunophenotyping staining – performed by Jelica Mehic (Research Technician; Lab Member)
- Mass Spectrometry - performed by Marybeth Creskey and Dr. Terry Cyr; Mass Spectrometry Laboratory CBE, BGTD, HPFB, Health Canada, Ottawa, ON, Canada
- NanoSight (NS300) - NTA performed at the Nanomedicines Laboratory, CBE, BGTD, HPFB, Health Canada, Ottawa, ON. Help and assistance by Grant Frahm.
- Flow cytometry –Andrew Stalker (Flow Cytometry Manager) CBE, BGTD, HPFB, Health Canada, Ottawa, ON, Canada, assisted in running the samples.

Research Funding: Genomics Research and Development Initiative Phase VI (2014-2019) obtained by Dr. Michael Rosu-Myles. Genomics Research & Development Initiative (GRDI) Phase VII (2020-2025) was obtained by Dr. Jessie R. Lavoie.

Thesis Advisory Committee Members:

- Dr. Lisheng Wang
- Dr. Michael Rosu-Myles
- Dr. Caryn Ito
- Dr. Marjorie Brand
- Dr. Jessie Lavoie

Abstract:

Background: The focus of this study was to investigate how producing human bone marrow (hBM) derived mesenchymal stromal cell (MSC) extracellular vehicles (EVs) in a high purity isolation system would affect their established characterization criteria and address the validity of these methods of EV production. Additionally, we set out to functionally characterize the hBM-MSC-EVs for their identified immunomodulatory ability while also assessing the presence of novel MSC-EV marker NRP1 identified by our group to further affirm its validity as a functional MSC-EV identity marker.

Methods: Each hBM-MSC-EV donor was cultured in a hollow-fiber bioreactor system in non-stimulating serum/xeno-free conditions for 25 days to produce EVs persistently under quiescent conditions to characterize the hBM-MSC-EVs in their native form. EVs were isolated by traditional PEG-based precipitation for preliminary characterization to monitor bioreactor production wherein they were characterized using multimodal tangential flow filtration coupled with fast protein liquid chromatograph (FPLC) size exclusion/high-affinity purifications to obtain the final highly purified EV sample. Additionally, functional analysis of their immunomodulatory ability, EVs and MSCs were incubated with activated peripheral blood mononuclear cells (PBMCs) as an *in-vitro* model to evaluate their potency.

Results: The hBM-MSC-EVs produced from the bioreactor system showed consistent characterization in accordance with the MISEV2018 establish criteria. We were also able to demonstrate their functional ability by observing statistically significantly immunomodulatory ability of activated PBMCs equivalent to native MSC ability. We were also able to validate the present of NRP1 on all hBM-MSC-EV samples produced confirming its validity as a MSC-EV marker.

Conclusion: The significance of the results obtained from this study confirms the production of MSC-EV using a bioreactor and high purity isolation for obtaining consistent MSC-EVs for downstream investigation. Additionally, we were able to demonstrate the significance of MSC-EVs on MSC signaling for immunomodulation by showing equivalent functional potency when tested *in-vitro*. These results contribute to further understanding the biological attributes of MSC-EVs and contribute to the validation of currently established characterization guidelines.

List of Abbreviations:

| | |
|---|---|
| Human Bone Marrow | hBM |
| Bone Marrow | BM |
| Coronavirus Disease of 2019 | COVID-19 |
| Graft-vs-Host-Disease | GvHD |
| Mesenchymal Stromal/Stem Cell | MSC |
| Endosomal Sorting Complexes Required For Transport | ESCRT |
| Intraluminal Vesicles | ILVs |
| Extracellular Vesicle | EV |
| Small Extracellular Vesicle | sEV |
| Size Exclusion Chromatography | SEC |
| Neuropillin-1 | NRP1 |
| Binding Affinity Chromatography | BAC |
| Medium Extracellular Vesicle/Large Extracellular Vesicle | mEV/lEV |
| Catalogue # | CAT# |
| RoosterBio | RB |
| Dulbecco's Phosphate Buffered Saline | D-PBS |
| Phosphate Buffered Saline | PBS |
| Fetal Bovine Serum | FBS |
| Ethylenediaminetetraacetic acid | EDTA |
| Multivesicular Body | MVB |

| | |
|---|---|
| Fast Protein Liquid Chromatography | FPLC |
| Tangential Flow Filtration | TFF |
| Peripheral Blood Mononuclear Cells | PBMC |
| International Society of Cell Therapies | ISCT |
| Polyvinylidene Fluoride | PVDF |
| Minimal Information for Studies of Extracellular vesicles 2018 | MISEV2018 |
| Fluorescent Activated Cell Sorting | FACS |
| Carboxyfluorescein succinimidyl ester | CFSE |
| Coefficient of Varience | CoV |
| 4-(2-hydroxyethyl)-1-piperazineethanesulfonic acid | HEPES |
| Tandem Mass Tag | TMT |
| Polyelthyene Glycol | PEG |
| Sodium Hydroxide | NaOH |
| Column Volume | CV |
| Extra-Capillary Space | ECS |
| KiloDalton | kDa |
| EV containing Medium | ECM |
| International Society of Extracellular Vesicles | ISEV |
| Nanoparticle Tracking Analysis | NTA |

Table of Contents

**Dedication:** This thesis is dedicated to my grandmother, who has always gone above and beyond her responsibilities to support me in my academic career. I am truly grateful for her support and guidance.

## Chapter 1: Introduction

### Mesenchymal Stem/Stromal Cells (MSCs):

Mesenchymal stromal cells are a multipotent stem/stromal cell population postulated with the capacity to differentiate into mesoderm lineages (adipocytes, osteocytes, and chondrocytes) as well as differentiation potential for myogenic lineages. (1-3) First identified by A.J Friedenstein in 1968 as a non-hematopoietic stem cell population present in the bone marrow. (4) Friedenstein's work on bone marrow confirmed the reserve of stem cells able to support proliferation and bone formation with a unique progenitor population. (4) These bone marrow progenitor cells were initially investigated for their osteogenic potential but were later identified with the ability to also support chondrocyte and adipocyte development in the 1970s. (5) Known as bone marrow stromal cells, they were later affirmed as a unique stem cell population and coined as "mesenchymal stem cells" by Arnold I. Caplan in the early 1990s. (6) Since then, profound evidence of MSCs ability has revealed these cells do not act in the classical mechanism associated with "stem cells" wherein traditional stem-like cells perform their function through the differentiation and regeneration of a particular cell type to repair injured tissue. (7, 8) While MSCs in particular have differentiation and regenerative potential, investigation of their biological activity showed they primarily exert their function through cellular signaling and secretion of a range of bioactive compounds.(9) Caplan himself in 2017 proposed a re-evaluation of the nomenclature associated with MSCs from "mesenchymal stem cells" to "medicinal signaling cells" as a result of their bioactive behavior. (10) Modern investigation of MSCs in regenerative medicine has concluded these cells display significant potential when processed *ex vivo,* however, when re-introduced *in-vivo,* it is still uncertain if they behave as observed in a laboratory setting. (11-13)

Their identification in a diverse range of tissues suggests they have native potential to migrate in vivo and can contribute to their observed ex vivo signaling mechanisms. (13) While initially identified in the bone marrow at a high abundance, MSCs are prominent in a variety of tissue types with varying levels of abundance including; adipose, umbilical cord, peripheral blood, and even dermal tissue. (8, 14, 15) The biological potency of the MSCs can dependent on the tissue of origin. MSCs derived from tissue sources closer to embryonic nature such as placental tissue, umbilical cord or amniotic fluid/membrane have been characterized with a higher potential for *ex-vivo* expansion before reaching senescence compared to more mature tissue sources such as adult bone marrow or adipose tissue. (16, 17) However, in some instances the isolation method from these tissue has also been shown to influence their proliferative potential. (17) Notably, explant isolation where the primary tissue sample is cultured on a treated tissue culture surface to allow for migrating adherent attachment of the MSCs compared to non-adherent tissue sub populations (Ex. Non-adherent bone marrow hematopoietic stem cell in a bone marrow sample) or enzymatic digestion isolation wherein the tissue sample is pretreated with a proteolytic enzyme to digest the non-cellular tissue components wherein the single-cell suspension is washed and then plated in treated culture surface to allow for adherent MSC attachment will affect their population doubling time. (16, 18)

**Mechanism of Action for Mesenchymal Stromal Cell Function:**

Increasing evidence and investigation into the function of MSCs have shown they support the potential for a diverse range of functions including tissue repair and immunomodulation achieved through complex signaling consistent with cell-to-cell contact as well as secreted components. (19) The functionality of MSCs has not been completely outlined; however, it is understood the

mechanics of action focuses on the paracrine effect through the deployment of secreted factors that affect the key regulators of cell survival and immunomodulation, and proliferation *in vivo*. (20) For cell survival and wound healing, MSCs can detect the chemical gradient of signaling factors (ex. bFGF, SDF-1, Osteopontin, and TGF-b) of injured cells such as endothelial cells, macrophages, fibroblasts, and keratinocytes to induce homing migration to the site of injury. (21, 22). MSCs are then capable of secreting a milieu of growth factors (ex. HGF, VEFG, PDGF, EGF, and FGF) as well as cytokines such as interleukins to promote cell survival. (20, 23) Additionally, through their ability to home and respond to their environment, MSCs are capable of targeted immunomodulation. (24) This immunomodulatory potential has been demonstrated in literature as a combination of cytokine-dependent and independent signaling. Cytokine-dependent immunomodulation has been characterized to functionally target T cells, B cells, natural killer cells, macrophages, and monocytes/dendritic cells (DCs) through the secretion of interleukins to target anti-inflammatory signaling of each cell type. Specifically, MSCs will neutralize the monocytes and dendritic cells pro-inflammatory signaling through secretion of IL-6 and IL-10 resulting in inhibition of monocyte and dendritic cell maturation and transitioning them to an immune-regulatory phenotype where a positive feedback loop of immune cell produced IL-10 supports the anti-inflammatory state. (24, 25) Suppression of T cells by MSCs has been when characterized through the combinatory secretion of anti-inflammatory interleukins, TGF-b1 as well as IDO to neutralize FOXP3 signaling preventing T cell induction. (26, 27) Cytokine independent immunomodulation also significantly contributes to the MSCs functional ability through direct cell-to-cell contact. MSCs will present surface proteins such as integrins, intracellular/vascular adhesion molecules (ICAMs/VCAMs), and toll-like receptors (TLRs) to

directly bind T cells disrupting TCR activation and inhibition of Notch-dependent T cell activation. (26, 28)

**Application of MSCs Immunomodulatory Ability:**

Clinical studies have focused on bone marrow-derived MSCs (BM-MSCs) due to their potency, abundance in the bone marrow compared to other sources, stability as primary cells under manipulation, and low immunogenicity following transplantation. (29) MSCs have longstanding support from clinical experimentation to validate their use in clinical applications, most notably their function as an immunomodulatory effector for clinical treatment of systemic inflammation and autoimmune diseases such as graft-vs-host disease (GvHD), sepsis, multiple sclerosis (MS) and even COVID-19 induced acute respiratory distress syndrome. (19, 30-33) Most notably, is the use of MSCs for treatment of steroid-refractory/resistant Graft-vs-Host Disease. Chronic GvHD occurs with an alloreactive response and system immune dysregulation. Donor T cells present in the donor bone marrow undergo vascular endothelial activation resulting in inflammatory activation with antigen presentation and thymic dysregulation. The imbalance of regulatory elements results in depletion of T regulatory cells function responsible for adaptive immune response. Repair mechanisms of the donor lymphocyte populations result in the development of chronic inflammation. The therapeutic intervention has been assessed by targeting key signaling factors associated with the immune response to foreign infection such as (TNF-a, IFN-y, IL-2, and Stat proteins) and their downstream effects such as NFkB and TLR cascade loops as part of the inflammasome allows for attenuation of the GvHD response. (34, 35) MSC's ability to directly regulate each immune cell subset as well as target the described key signaling factors through secretory dependent and independent signaling have resulted in their adaptation as a biological therapy for GvHD. The underlying success of MSC infusions following hematopoietic stem cell

transplantation to combat severe complications such as graft-vs-host disease or organ transplant rejection is observed with countless clinical trials observed with the success of reducing inflammatory incidents and improving graft survival. (34, 36-38) Several pharmaceutically investigated products such as *Prochymal*/*Remestemcel-L* have been approved by governing agencies such as Health Canada for pediatric applications.

It is noted that this immunomodulatory potential has also been observed to be beneficial for the treatment of other medical issues related to immune dysregulation, such as sepsis. As one of the leading causes of death of hospitalized patients, the assessment of MSCs as a biological treatment based on their immunoregulatory ability was validated by extensive review. Similar to immunological inflammation, sepsis is the result of systemic infection of the body by a bacterial pathogen resulting in dysregulation of the innate immune response. (39) MSCs have been shown to target the pro-inflammatory environment of sepsis pathological infection with both paracrine actions of secreted factors and TLR receptor-mediated cell contact to suppress inflammatory phenotype. (39, 40) Specifically, MSCs will secrete inhibitory factors (ex. IL-6, IL-10, IDO, and TFG-b) to pro-inflammatory mediators of sepsis such as; TNF-a, interleukins (ex. IL-2, IL12, and IL17/18) and interferon-y to downregulate the hyper-inflammatory feedback loop of bacterial infection.

**Stem-like Properties of MSCs for Regenerative Medicine.**

Separate to its influence on the immune system, MSCs have also been assessed for other more traditional stem-like regenerative potential with their differentiation ability, progenitor cell fusion potential, and trans-differentiation ability to repair injured tissues such as muscle/skeletal tissue,

myocardium, and neuronal cells respectively. (41-43) MSCs differentiation potential for chondrocytes as well as myogenic lineages has been proven used in cartilage and smooth muscle regeneration therapy by transplanting MSCs to injured sites to promote native tissue repair but also potentially repopulate the damaged tissue through differentiation. (1, 7, 44, 45) Transplantation of differentiated MSCs is still not recommended due to complications associated with the changes in the differentiated MSCs immunogenicity to cause an immune reaction but also the heterogeneity of the differentiated population. (46) It is not readily identified *in vivo*, however, *in vitro*, MSCs have exhibited the ability for cell-to-cell fusion as a means to integrate into the tissue microenvironment and promote tissue homeostasis. (47) Through entosis, MSCs can fuse with neighboring cell types through engulfment as a means to re-establish tissue function during injury. Furthermore, MSCs are also capable of transdifferentiating as opposed to a permanent state of cell differentiation into a separate mature cell type. Seen especially in instances of cardiac and neuronal repair. MSCs are able to partially differentiate from their progenitor state into a hybrid cell state to promote regeneration of the localized environment. (48, 49) This hybrid state is described as the transient expression of tissue specific markers.(50, 51) Through investigation into the complexity of MSC signaling, genetic modulation and the production of soluble factors, it is understood that beyond the present of cytokines, chemokine and soluble proteins, it has been identified that secreted extracellular vesicles contribute significantly to MSCs regulatory ability and mechanism of action.

**History of Extracellular Vesicles:**

Similar to MSCs, extracellular vesicles were first identified in the late 1960s by HC Anderson. While investigating the cartilage matric tissue of mice and were described as variably sized from

300A to 1 micron in diameter and membrane-bound. (52) Following this initial discovery, they were commonly identified in studies investigating the structural dynamic of material samples most often under electron microscopy due to their nanoscale size. In 1975, the first comparison of these vesicles to virus-like particles from multivesicular bodies of epithelial cells revealed their identity as a normal cell component. (53) From there, EVs were actively investigated to identify their molecular production and release mechanism where Johnstone et al, were able to demonstrate that by comparing reticulocytes to mature cells that do not express several membrane-associated proteins including transferring and ATPase, that EVs were not produced by mature cells and were dependent on the membrane proteins for release. (54) With modern technology, the investigation into the biogenesis of EVs is now mechanistically characterized and they are no longer considered a cellular byproduct but are actively, and specifically packaged for critical cell functions. (55) The described function of EVs observed through countless investigations of vesicles produced from different cell types is to facilitate the transfer (albeit, targeted or untargeted) of proteins, mRNA, small RNAs, and biochemical signaling molecules via a protective and complex lipid bilayer between cells in a paracrine or endocrine manner.

**Biological Production of Extracellular Vesicles:**

Extracellular Vesicles are a secreted membrane-bound vesicles produced by cells through the endosomal system within the plasma membrane. While not completely understood, the biogenesis of EVs can occur by two molecular mechanisms known as the endosomal sorting complexes required for transport (ESCRTs) protein dependant or independent pathway. (56) The ESCRT dependent biogenesis of EVs occurs with the processing of intraluminal vesicles (ILVs) in the multivesicular body (MVBs) with stepwise recruitment of the ESCRT family of proteins to process

the ILVs for ubiquitination of proteins for sorting, assembly of the early endosome, intraluminal budding and formation of the EVs.(Figure B1) EVs are also produced independently of the ESCRT protein factors, however, these independent mechanisms of production are highly dependent on the cell type for the detailed mechanism of biogenesis. Regardless of the mechanism of production, once the MVB containing the ILVs is matured, the vesicles are actively secreted through transportation by cytoskeletal motor transport and the RAB family of proteins for trafficking and vesicle secretion (56, 57)

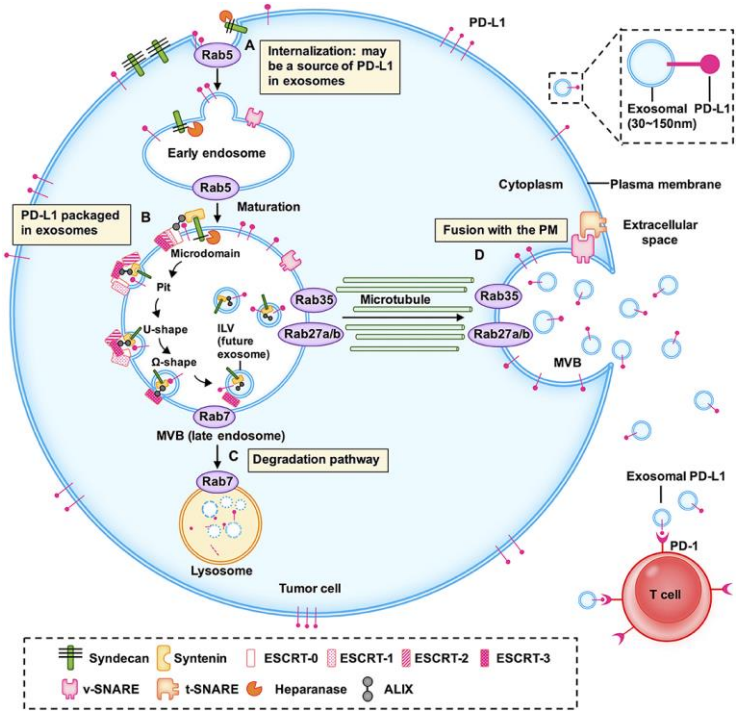


Figure B1: ESCRT dependent signaling pathway for production of small extracellular vesicles. (90)

**Mechanism of Action for Extracellular Vesicles and Cellular Signaling:**

The functional investigation of EVs has shown their membrane composition with embedded transmembrane receptors in addition to specific packaging of proteins, DNA and RNAs are essential to their ability to deliver their cellular signaling. The mechanism of action for EVs flows

either direct signaling, membrane fusion, or endocytosis. (56) Depending on the parental cell, the molecular surface profile of the EVs contains cell-identifying receptors capable of targeted receptor-ligand interactions for direct signaling like other soluble factors. Additionally, the presence of a membrane bilayer serves a dual purpose of protecting delicate cargo such as DNA and RNA while also providing an alternative means of delivery of internal cargo and receptor proteins via membrane fusion of the EVs with the recipient cells membrane. (58, 59) EVs can also function through bulk uptake of secreted EVs like a chemokine response wherein EVs are up taken through endocytosis by the responding cell. (60) With this information supporting EVs importance for cellular signaling, cell-based investigations of paracrine action have re-evaluated their understanding to include the impact of cell-produced EVs contributing to the observed response. (60, 61) Investigation of MSC-derived EVs has shown their molecular profile containing proteins and RNA  EV cargo contain a comparable distribution of anti-inflammatory cytokines and micro RNA  specific for immunomodulation to that observed in the MSC secretome. (60-62) With new light on the impact of EVs on basic cell function, the current focus of EV-related work is understanding the diversity of EV functionality including exploiting their observed ability to mimic cell function as a "cell-free" mechanism of investigation cellular signaling. (14, 55, 56)

**Characterization of Extracellular Vesicles:**

In conjunction with increase interest in EVs also harbors the requirement of characterization and standardization of evaluating EVs to provide more scientific evidence to support EV work. The International Society of Extracellular Vesicles (ISEV) highlights established criteria with respect to the characterization of EVs for research and therapy. Specifically, the "*minimal information for studies of extracellular vesicles 2018*" (MISEV2018) position paper outline the

requirements for EVs with respect to identifying the particles' overall size, particle composition, functional assessment, EV specific characterization criteria, and recommendations on methods of isolated these particles follow cellular biogenesis. (63)

The use of "exosomes" has not been explicitly defined with regards to subtype characterization and is currently used interchangeably with the term extracellular vesicles. Extracellular vesicles are currently classified into two main categories with "small EVs" (sEVs) less than 200nm in diameter while "medium/large EVs" (m/lEVs) are considered greater than 200nm in diameter. Small extracellular vesicles have been historically classified as "exosomes", wherein medium/large EVs encompass a larger variety of vesicles types including; apoptotic bodies, microvesicles, and oncosomes. (Figure B2) The composition of EVs displays a selection of established protein markers most notably the presence of tetraspanins such as CD63, CD81, and CD9 as well as the presence of MVB processing proteins such as syntenin, Alix, and ESCRT associated proteins. (57, 63)

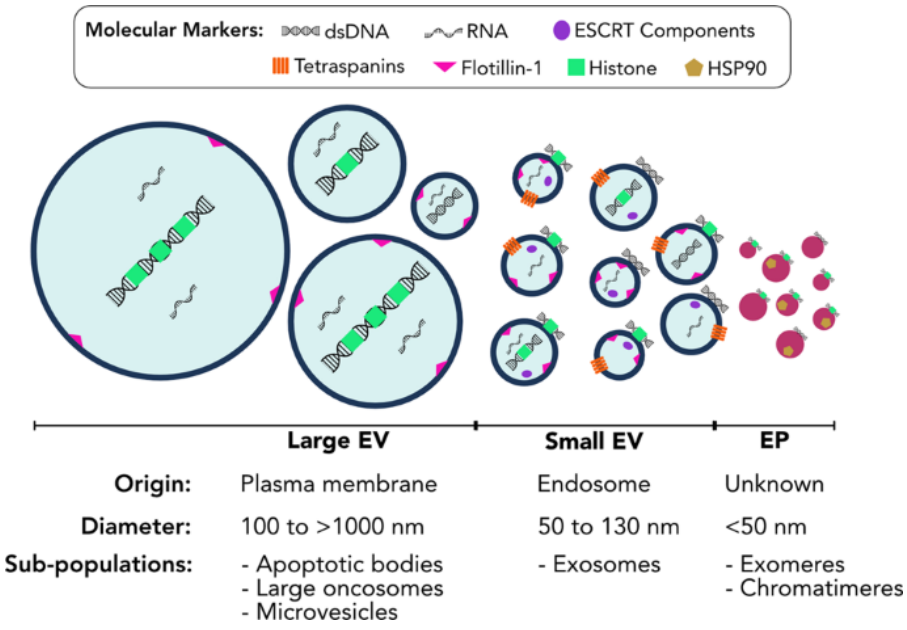


Figure B2: Main classifications of extracellular vesicles comparing size and cargo of large EVs, small EVs and extracellular particles (EP)(89)

Isolation of EVs done by several methods results in a variety of outcomes, in the early stages of EV discovery main mechanism of EV isolation was differential or high-speed centrifugation of sample material to try and pellet the vesicles based on their size and density. This was a cost-effective means of isolating nanoscale particles however it would often result in result co-isolation of contamination of non-EV particles with similar chemical compositions such as apoptotic bodies, protein aggregates, vLDL particles, and microvesicles. (63, 64) Additionally, high-speed centrifugation also has the potential for protein and RNA degradation under sheer stress. The exploitation of EV membrane chemical properties has also been investigated by chemical-based isolation such as precipitation. With a similar membrane composition to that of virus particles, virus-like isolation methods were assessed for their ability to purify EV populations. (64) The addition of water excluding detergents such as polyethylene glycol (PEG) or dextran (DEX) has been used to bind the EVs in aqueous solutions and destabilize their interactions with water to essentially precipitate or "crash" the particle out of solution. (65) This isolation method benefits from improved specificity of particle characteristics but is not compatible with a biological system where other similar composed molecules such as virus-like particles also co-exist. (66) Highly specific means of purification have been developed to negate these issues such as ultrafiltration, size exclusion chromatography, and binding affinity chromatography and are considered to be high specificity methods of isolation compared to other approaches such as PEG precipitation and ultracentrifugation. (63) Ultrafiltration consists of filtering the EV-containing samples through one or more membranes (i.e. Tangential flow filtration) with a specific pore size restriction in order to remover larger contaminants by size since EVs can be characterized by their vesicle diameter such as described by the ISEV2018 guidelines. Additionally to the size restriction, samples are often simultaneously buffer exchanged which entails adding additional contaminant-free buffer solution

to dilute out molecular contaminants known as diafiltration. Size exclusion chromatography (SEC) and binding affinity chromatography (BAC) sometimes combined as multimodal chromatography have been identified as the purest method of EV isolation. (63, 67, 68) Specifically, multimodal chromatography combines the pore cutoff exclusion of SEC with high affinity binding resin of (BAC) to purify exosomes by size and remove similarly sized particles with solubilized proteins., (67, 69, 70) Additionally, EVs produced and isolated under serum/xeno-free conditions are preferred for investigation of cell specific EV characterization due to the potential for xenogeneic contamination of particles from sources such as animal derived serums/ matrix complexes since most bio-fluids especially serums for standard culture contain material derived exosomes.

**Neuropilin-1: Functional and Biological Relevance**

Biomarkers of MSCs and MSC-EVs have been investigated as a means of understanding their heterogeneity and function. Our lab has previously identified and validated the Neuropilin-1 (NRP1) protein as a novel marker for hBM-MSC and MSC-EVs ex vivo. (59, 71) NRP1 was originally identified by Takagi et al as a membrane-associated glycoprotein by the production of anti-NRP1 antibodies (known as A5 at the time) in Xenopus tadpoles with a suggested function involved in target recognition of the optic nerve due to its identification in the optic tectum. (72) The entire neuropilins family of proteins was then characterized by Kolodkin et al. in 1997 as a semaphorin type III receptor, with its primary function as a chemotropic cue for axon guidance. (73, 74) As a type 1 transmembrane protein initial expression was observed on several distinct neuronal populations. (75) Since its initial discovery, the role of NRP1 has expanded beyond its neurological association, and is now established as a multifaceted, single-pass transmembrane,

glycoprotein with functional signaling in the realms of; immunomodulation, neuron development, angiogenesis, and physiological development. Its variable expression across a multitude of immune cell subtypes such as macrophages, dendritic cells, B cells, and T cells has supported its role in immunological response signaling. (75-77)

**Neuropilins: Signaling Pathway:**

The NRP family of proteins consists of two main transmembrane proteins known as Neuropilin-1 (NRP1) and neuropilin-2 (NRP2). Both proteins share the same extracellular structure containing 5 extracellular domains with a single intracellular binding domain. Comparison of NRP1 and 2 dictates less than 50% overall sequence homology with a splice peptide sequence in the C domain of the extracellular portion allowing for the soluble transformation of both NRP1 and NRP2 genes to generate their soluble protein counterparts known as sNRP1 and sNRP2 respectively. The primary role established for NRP proteins is the binding of semaphorin class III members primarily the VEFG family of proteins. For angiogenic regulation, NRP1 will bind several independent pathways such as; intracellular kinases such as ABL1 to promote extracellular matrix binding for the initial development of the vascular endothelium, semaphorin (SEMA3A) binding for lymphatic endothelium promotion, and VEFG-A as a co-receptor of VEGFR. (78) Following co-binding, the NRP1-VEGFR complex will induce intracellular kinase (i.e. MAPK, ATK, and ERK) activity promoting transcription gene activation of actin development for vessel branching thought VEGF signal cascade. (79-81) NRP1 is known to bind a series of additional growth factors such a TGB-beta and Argonaut family of proteins to diversify its signaling role with respect to tumor vascularization and tumor promotion. (76, 81)

**Neuropilins: Clinical Significance of Immunomodulatory Potential:**

NRP1 was determined to be particularly important with respect to immune system signaling and the immunological response. (37, 77) Through co-localization on the various immune cell subtypes, NRP1 is essential to stabilizing the formation of the immunological synapse between immune cells particularly T cells and DCs to establish the primary immune response. (Figure B3) More specifically, the role of NRP1 in T cells has been observed to play an immunosuppressive effect on activated T cell populations. These results have pressed additional investigation into the implication of NRP1 on graft survival following transplant and mechanistic investigation of T cell-mediated graft rejection. (37) The expression and accumulation of NRP1 in T cells were observed to suppress their overall proliferative response resulting in anti-inflammatory signaling and attenuation of the immune system.

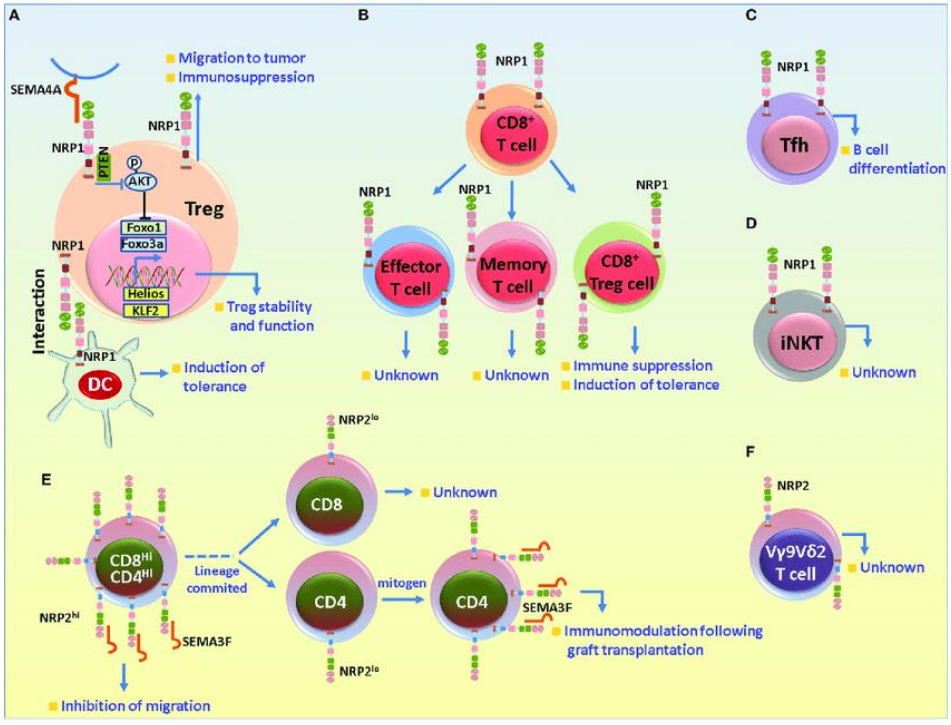


Figure B3: Functional transfer and binding of NRP1 in immunological signalling (91)

## Chapter 2: Research Objectives and Hypothesis:

**Hypothesis:** *Highly purified hBM-MSC-EVs capable of immunosuppression of activated peripheral blood mononuclear cells will present NRP1.*

**Rationale:** Our group has previously identified NRP1 as a novel MSC/MSC-EV marker. It is well established that the active production of EVs selectively packages proteins in EVs in order to exert a signaling function. The specific packaging of NRP1 on MSC-EVs compared to other established MSC-associated proteins would suggest NRP1 dictates a supported function of MSC-EVs. The NRP1 protein is associated with immunomodulation and suppression of expressing immune cells activity. It has also been shown that horizontal transfer of NRP1 for adaptive immune response regulation significantly contributes to immunomodulation. NRP1 is also associated with the immunomodulatory potential of tumor cells for evading the system's immune response. Profound literature support would suggest that if NRP1 is present on MSC-EVs they should demonstrate immunomodulatory potential as well.

**Objective:**

1. Assessment of hBM-MSCs in the non-stimulating bioreactor environment to confirm maintenance of MSC population.
2. Production and characterization of EVs produced from hBM-MSCs in a bioreactor.
3. Characterization of NRP1 presentation on the bioreactor produced hBM-MSC-EVs.
4. Functional assessment of bioreactor-produced hBM-MSC-EV for immune suppression of active immune cells.

## Chapter 3: Methodology

### Cell Expansion and Characterization:

### hBM-MSC Isolation:

Human bone marrow mesenchymal stromal cells (hBM-MSCs) were derived from the bone marrow of four healthy male donors which were generated by the company RoosterBio (RB) Inc. (Frederick, MD, USA) under informed consent. The purchased hBM-MSC cultures were fully characterized according to the International Society for Cell and Gene Therapy's (ISCT) minimal criteria. (8) Our laboratory further performed hBM-MSC characterization for the expression of surface markers by flow cytometry and the mesoderm trilineage differentiation potential (adipocytes, osteocytes, and chondrocytes). The hBM-MSC cultures from the four donors were expanded from initial purchase at passages 0–1 to generate working cell banks at passages 1–2 as per RoosterBio Inc.'s protocol with slight modifications, as previously described in {Gobin, 2021 #4} hBM-MSCs were grown in RoosterBio MSC complete media (RoosterBasal-MSC and RoosterBooster-MSC, RoosterBio CAT#KT-001)

**hBM-MSC Thaw and Expansion from Liquid Nitrogen Storage**:

For each of the 5 different donors obtained commercially through (RoosterBio, CAT# MSC001) vials of hBM-MSCs were each retrieved from liquid nitrogen storage to achieve a total cell count of approximately 20 million cells per donor. Vials were then thawed in a 37°C water bath until the frozen cell pellet became dislodged from the vial bottom. The vials were then transferred aseptically to a biosafety cabinet for processing. For each donor, the vial's contents containing the cells pooled and transferred to a 50mL tube (Corning, CAT# 430290). To equilibrate the cells, 40-

50mL of pre-warmed RoosterBio MSC complete media was added dropwise to each bottle containing cells. The cell suspension was mixed and a 20uL aliquot was taken for trypan blue cell count and viability assessment.

**Trypan Blue Viability Assessment and Cell Count:**

To determine the viability and cell concentration of cell samples following thawing or harvest. 20uL of cell suspension was transferred to a 0.5mL centrifuge tube (Eppendorf, CAT# 022431005) and diluted 1:2 with 20uL of 0.4% trypan blue (Invitrogen, cat. #T10282), the cell suspension was mixed briefly by gentle pipetting before 20uL was injected into cell counting slide (Nexcelom CAT# PD100) and the slide was measured using the Cellometer Auto 1000 brightfield cell counter (Nexcelom Bioscience). Slide focus was manually adjusted until the cells were in view with clearly defined edges. Counts were taken in duplicate unless the coefficient of variances (CoV) was greater than 25% wherein an additional cell count was conducted for accuracy.

**Seeding and Expansion of hBM-MSCs in CS10 Stacked Cell Culture Flasks:**

Aseptically, following cell count to confirm the number of viable cells exceeded 20 million cells total, the cell suspension containing the 20 million cells was split into 3 bottles of pre-warmed 37°C RoosterBio MSC complete media, and the cell suspension was mixed by gentle inversion. Additionally, in order to visualize the expansion of the hBM-MSCs, one tissue culture treated T-175cm$^2$ flask (Corning, CAT# 431080) was seeded at an identical seeding density of 3145 cells per cm$^2$. The 3 bottles of cell suspension were transferred into a pre-warmed tissue culture treated CS10 stacked flask (Corning, CAT# 3271) by pouring contents of the bottle into one of the fill

ports. Once all 3 bottles containing cell suspension were transferred the fill ports were capped and the flask was turned on its side to allow for equal distribution of cell suspension between each chamber. The flask was then turn on its back and then returned to a horizontal position to distribute the volume of each chamber across its attachment surface before being returned to the incubator. The additional T-175cm$^2$ flask was placed in the same incubate for visualization during expansion. After overnight incubation in the incubator (ThermoFisher Heracell 150i CAT# 51026529) the T-175cm$^2$ flask was removed daily and visualized using the Leica microscope on objective 10x to confirm cell attachment and assess the seeding density by confluency of the attachment surface. Cells were allowed to expand in the CS10 and T-175cm$^2$ flask until the attachment surface displayed a visually estimated confluency of 80-90% of the total area indicated the CS10 stack flask should have a total cell volume in excess of 100 million cells total.

**Harvesting the hBM-MSCs from the CS10 for Bioreactor Production and ISCT MSC Characterization:**

Following the expansion of the CS10 flask, once the T-175cm$^2$ visualization flask indicated the harvesting confluency of 80-90%, the CS10 was transferred to the biosafety cabinet aseptically for hBM-MSC harvesting. One fill port was opened and the spent medium was aspirated wherein 200mL of pre-warmed 0.25% Trypsin/EDTA (Gibco, CAT#252000-72) poured into the CS10 and the flask was capped and the volume of 0.25%Trypsin/EDTA was distributed evenly across the chambers before being returned to the incubator to incubate at 37°C for 6-8 minutes to allow for cell detachment. The harvesting process was repeated in parallel with the T-175cm$^2$ flask to indicate when cell detachment had occurred. Following confirmation of cell detachment, the Trypsin/EDTA cell suspension in the CS10 was aseptically returned to the biosafety cabinet, and

the harvesting activity was quenched with 200mL of pre-warmed D-PBS (Gibco, CAT#14190250) containing 2% of MSC-screened FBS (Hyclone, cat.#SH300700.03 M). The total cell suspension (400mL) was then transferred from the CS10 to a 500mL bottle (Corning, CAT#430282) and 20uL was taken for trypan blue cell count and viability assessment. The 400mL of cell suspension was then transferred to 10 x 50mL centrifuge tubes (Corning, CAT# 430290) and spun down at 200xg for 10 minutes to collect the cell pellets. Following the spin, the supernatant was aspirated and each pellet was re-suspended in 2mL of RoosterBio MSC complete media by gentle flicking and pipetting. The cell suspension was then pooled for a total volume of 20mL to be injected into the hollow fiber bioreactor system. One million cells were set aside for flow cytometry assessment of the hBM-MSCs for their established ISCT Surface Identity Markers.

**Inoculation of hBM-MSCs in the FiberCell Systems Hollow Fibre Bioreactor for EV Production:**

Prior to the expansion of the hBM-MSCs the hollow fiber bioreactor (FiberCell Systems, CAT# P3202) was first prepared for cell seeding as per the manufactures pre-equilibration procedure. Briefly, the hollow fiber reservoir caps and tubing were autoclaved for sterility prior to use. In the biosafety cabinet, the media reservoir bottle, cap tubing, and hollow fiber cell bioreactor cartridge (20-kDa MWCO, 4000 $cm^2$, high flux polysulfone fiber type; FiberCell Systems, CAT# C2011) were assembled wherein 250mL sterile D-PBS (Gibco, CAT# 14190250) was added to the reservoir and 20mL was added to the cartridge extra capillary space (ECS) to begin equilibration of the PVDF fiber capillaries. The assembled bioreactor was placed in the incubate pump at a flow rate of 22 for 3 days. Following equilibration, the PBS was removed aseptically and replaced with RoosterBio MSC media for 24 hours, wherein it was aseptically removed and replaced with

RoosterBio MSC complete media for 24 hours until the cells were ready for inoculation. Prior to injection of the 20mL of cells (*Harvesting the hBM-MSCs from the CS10 for Bioreactor Production and ISCT MSC Characterization*) from the bioreactor was replaced with fresh RoosterBio MSC complete media and cells were injected into the extra capillary space using a 20mL syringe (BD Bioscience, CAT# 309661) attached to one of the fill ports. Following injection of the cells into the ECS, the bioreactor was laid on the front side for 30 minutes then the backside for an additional 30 minutes in the incubator to allow the cell suspension to settle and attach to the membrane capillaries. The bioreactor was then set into the incubator pump at a pump rate of 22 for 3 days for the cells to adapt to the bioreactor microenvironment. The ECS was then transitioned to RoosterCollect-EV (RoosterBio, CAT# M2001) to begin serum/xeno-free long-term EV production. From days 3–17 of the 28-day cell inoculation period into the bioreactor, the media volume in the extracellular capillary space was 250 mL and circulates at a system flow rate of 25. After day 17, the media volume was doubled to 500 mL with the same flow rate to supplement the system with glucose.

**Harvesting EVs from hBM-MSCs in the Hollow Fibre Bioreactor System:**

To collect the EV-containing media from the hollow fiber bioreactor system, the bioreactor was transferred to the biosafety cabinet for aseptic handling. The side ports of the bioreactor capsule were closed to prevent media flow through the system during processing. A new 20mL syringe was attached to the right fill port of the ECS and a new syringe containing 20mL of pre-warmed RoosterCollect-EV media was attached to the left ECS fill port. The new RoosterCollect-EV media was pushed into the ECS allowing the EV-containing media to be pushed out of the ECS into the empty syringe for harvesting. Once the entire volume of fresh RoosterCollect EV was pushed into

the ECS and the EV containing media was pushed into the right syringe all the fill ports were closed and the media containing syringe was removed and contents were emptied into a 50mL centrifuge tube (Corning, CAT# 430290) and the EV containing media was spun down at 200xg for 10 minutes clear the media of cells or debris. The cleared media was then aliquoted into 4 x 5mL aliquots in 15ml centrifuge tubes (Corning, CAT# 430053) for storage at -80°C. The final harvest of EVs from hollow fiber bioreactor was done as described above with double-filtered D-PBS (Gibco, CAT# 14190250) to push out the EV containing ECM.

**Monitoring the Metabolic Condition of the Hollow Fibre Bioreactor System by Glucose, Lactic Acid, and pH.**

To determine the overall condition of the cells and metabolic rates, the bioreactor system was transferred to the biosafety cabinet for media sampling from the reservoir every 2 days to measure glucose and lactic acid levels in the system. 1 milliliter of media was taken from the reservoir to and transferred to a low binding 1.5mL centrifugal tube (Eppendorf, CAT# 022431021). 20uL was taken from the aliquot and added to a glucose strip and measured using the AccuCheck Meter (AccuCheck Guide Glucose meter, Model 930). 20uL of the media sample was added to a pH strip (Fisher Scientific 6.8-13, CAT# B60-SHTRG-065130-VPS) and compared to the visualization chart to ensure system pH was maintained in the 7.0-7.5 pH range for cell culture. Finally, the remaining media sample was frozen down at -20°C until it could be tested for lactic acid by plate-based assay. (Abcam, CAT# ab65331)

**Recovery of the hBM-MSCs for Post Bioreactor ISCT MSC Characterization:**

Characterization of the hBM-MSCs following 25 days of EV production in the hollow fiber bioreactor system was done to ensure maintenance of stem-like qualities and identity in accordance with the ISCT MSC minimal criteria. Following the final harvest of EV containing media (ECM) with double-filtered D-PBS as described above, the hollow fiber system was aseptically transferred to a biosafety cabinet where bioreactor side capsule ports were closed and the ECS was flushed with 40mL of pre-warmed D-PBS to wash the cells in preparation of Trypsin/EDTA cell harvest. Following attachment of new sterile 20mL syringes to the left and right ECS ports, 40mL of pre-warmed 0.25% Trypsin/EDTA solution (Gibco, CAT# 252000-72) was injected into the ECS and mixed back and forth between the attached ECS syringe to distribute the trypsin/EDTA solution in the capsule. The bioreactor system was returned to the incubator for 10 minutes. The bioreactor system was returned to the biosafety cabinet and the ECS was mixed back and forth to dislodge the trypsinized cells. Finally, the trypsinized cells were pushed out of the bioreactor capsule using 3 x 20mL injections of D-PBS and transferred the cell suspension to a 50mL centrifugal tube (Corning, CAT# 430290) where it was quenched with an equivalent volume of D-PBS containing 2% MSC-screened FBS and spun down at 200xg for 10 minutes. The cell pellet was re-suspended in of D-PBS (Gibco, CAT# 14190250) containing 2% of MSC-screened FBS (Hyclone, CAT# SH300700.03 M), and counted using Trypan Blue Viability Assessment (Trypan Blue Viability Assessment and Cell Count). One million cells were set aside for flow cytometry assessment of the hBM-MSCs for their established ISCT Surface Identity Markers (Immunophenotyping MSC Identity of hBM-MSCs by Flow Cytometry). The other cells were seeded in 24 well plates for trilineage differentiation assay (hBM-MSC Trilineages Mesoderm Differentiation Analysis), or spun down again at 280xg and re-suspended in CryoStor CS10 preservation media for liquid nitrogen storage (Stem Cell Technologies, CAT# 07930).

**Immunophenotyping MSC Identity of hBM-MSCs by Flow Cytometry:**

The expression of hBM-MSC surface markers set by the ISCT's minimal criteria for MSC characterization was analyzed using the BD Stemflow hMSCs Analysis Kit (BD Biosciences, CAT# 562245) according to the manufacturer's protocol. The hBM-MSCs were assessed for the panel of surface markers prior to inoculation in the hollow-fiber bioreactor and again after their 28-day incubation period. Collected cells were washed using D-PBS (Gibco, CAT# 14190250) containing 2% of MSC-screened FBS (Hyclone, CAT# SH300700.03 M) (i.e. flow buffer), counted, and suspended in 1 mL of flow buffer followed by a filtration step through a 40-µm cell strainer to remove potential cell clumps. A hundred microliters of cell suspension were then added to each flow tube ($0.5 \times 10^6$ cells per tube) containing the antibody or cocktail of antibodies of interest as well as the corresponding isotype controls. Each tube was incubated in the dark for 30 min at 4 °C after which the cells were washed two times with the flow buffer and the volume was brought up to 4 mL with the flow buffer and cells were centrifuged at 1100 rpm for 6 min at 4 °C. The supernatant was discarded and the pellet was suspended in 0.5 mL of flow buffer and analyzed by flow cytometry using the LSRII flow cytometer (BD Biosciences). Fifty thousand events per sample were collected and raw data were analyzed using FlowJo V10 (FlowJo LLC, Ashland, OR, USA). Additional identical antibodies from the BD Stemflow hMSCs Analysis Kit were purchased to analyze the expression of single CD34 and HLA-DR-stained cells.

**hBM-MSC Trilineages Mesoderm Differentiation Analysis:**

hBM-MSCs were assessed for mesoderm trilineage differentiation capacity after the incubation period in the hollow-fiber bioreactor system. For assessing hBM-MSC chondrogenic differentiation potential, StemXVivo human chondrogenic supplement 100X (R&D Systems, CAT# CCM006) was added to the StemXVivo chondrogenic base medium (R&D Systems, CAT# CCM005) according to the manufacturer's procedure. Two hundred thousand hBM-MSCs were pelleted and incubated with 0.5 mL of chondrogenic differentiation medium for 14–28 days. Adipogenic differentiation potential was achieved by first seeding hBM-MSCs in 24-well plates ($2.5 \times 10^4$/well) in RoosterBio complete medium for 3 days, and then switching the medium to the adipogenic differentiation medium (R&D Systems, StemXVivo Adipogenic Base (CAT# CCM007) and the StemXVivo Adipogenic Supplement 100X (R&D Systems, CAT# CCM011) for 14–21 days. Osteogenic differentiation potential was achieved by first seeding hBM-MSCs in 24-well plates ($5.0 \times 10^3$/well) in RoosterBio complete medium for 3 days and then switching the medium to the osteogenic differentiation medium (R&D Systems; StemXVivo Osteogenic Base (R&D Systems, CAT# CCM007) and the StemXVivo osteogenic Supplement 20X, (R&D Systems, CAT# CCM008) for 14–21 days. The culture medium was changed every 2–3 days for all three lineages using the corresponding inductive media and non-differentiated wells were kept as controls where a normal medium was used for the media change. Cells for all conditions were fixed with 4% paraformaldehyde in D-PBS (Gibco, CAT# 14190250) and stained for the presence of adipocytes using Oil Red O stain (Electron Microscopy Sciences, CAT# 26503-02), osteocytes using Alizarin S 0.2% Solution (Electron Microscopy Sciences, CAT# 26206-01), and chondrocytes using Alcian Blue 8GX (Sigma, CAT.#A5268-10G). Transmitted light images were taken using Zeiss Observer microscope using 10 and 20X objectives.

**EV Isolation: Precipitation based EV purification of EV hBM-MSC-conditioned medium collected from the hollow-fiber bioreactor system:**

To purify EVs, each 20-mL aliquot of the ECM harvested from the hollow-fiber system was processed by precipitation based on the Total Exosome Isolation Reagent. The frozen aliquot of 20 mL of ECM was thawed at room temperature on the day of use and processed immediately after thawing. The freshly thawed ECM was then mixed with 0.5 of the equivalent volume of Total Exosome Isolation Reagent (approximately 10 mL) (Invitrogen, CAT#4478359) and vortexed at the maximum speed (10) until the solution was homogenous. The sample was incubated overnight at 4 °C and was centrifuged at 10,000 × *g* for 1 hour at 4°C the next day. The supernatant was removed and the EV pellet was suspended in 1 mL of double-filtered D-PBS (Gibco, CAT# 14190250). For this study, the 20-mL ECM samples were collected daily; however, only the samples harvested at collection days 1–2 (start), days 13–14 (interim), and days 24–25 (end) were used for time point analyses of EVs.

**Diafiltration and Concentration of EV-rich hBM-MSC Media by Single Phase Tangential Flow Filtration:**

To generate a concentrated EV stock for downstream characterization and functional assessment, 90-110mL of ECM comprising all 25 days of EV production from the hollow fiber bioreactor was thawed overnight at 4°C in the fridge, once thawed the samples were mixed in a 250mL bottle (Corning) and diluted 1:2 in double-filtered D-PBS (Gibco, CAT# 14190250). The Minimate EVO Tangential Flow Filtration (Pall Life Sciences, OAPMPUNV) was assembled as per the manufacturer's recommendation using Masterflex L/S #16 Pharmed peristaltic pump tubing (Cole-

Parmer, CAT#RK-06508) and Masterflex high-pressure three-way stopcock connectors (Cole-Parmer, CAT# UZ-30526) and a PES 300kDa Omega Minimate TFF cartridge (Pall Life Sciences, CAT# OA300C12). The system was first flushed with 500mL of 18.2Ω double-filtered MilliQ water at 100mL/min, followed by a sanitization solution as per the manufacturer's recommendations (37°C pre-warmed 0.5N BioUltra NaOH (Millipore Sigma, CAT# 72068-100ML) in 18.2Ω double-filtered MilliQ water for 30 minutes at 50mL/min). Following sanitization, the system was drained and flushed again with 500mL of 18.2Ω double-filtered MilliQ water at 100mL/min. After draining the previous system flush, membrane equilibration was done by cycling 250mL of double-filtered D-PBS (Gibco, CAT# 14190250) for 30 minutes at 50mL/min. Finally, the system was drained, and the diluted EV sample was added to the reservoir by pouring down the side of the reservoir to prevent the introduction of bubbles. The system was cycled in a closed-loop for 5 minutes to ensure the cross-flow membrane pressure remained stable at 40-50mL/ min. To diafiltrate/concentrate the sample, a tubing clamp was tightened on the post cartridge retentate tubing to build the backpressure up to between 10-15 PSI and the filtrated was sent to waste. Diafiltration/concentration was continued until the desired volume was achieved 30-40mL. To retrieve the sample, all tubing clamps were removed and the system loop was closed and allows to run in the reverse flow direction for 5 minutes to normalize the solution through the tubing prior to collection at 50mL/min. A new 60mL syringe (BD Bioscience, CAT# 13-689-8) was added to the pre-reservoir retentate value and the loop flow direction was sent directly to the syringe to begin collection at 25-30mL mL/min. Once the entire sample was collected in the syringe, the bubbles were removed and the sample was capped and stored until ready for purification.

**hBM-MSC EV Isolation and Purification by Multimodal Binding Affinity Size Exclusion Fast-Protein Liquid Chromatography:**

To purify the EV sample of residual soluble biological contaminants (proteins, DNA, RNA), the sample was processed using the AKTAStart FPLC system (Cytiva Life Sciences, CAT# 29022094) with a HiScreen CaptoCore 700 chromatography column (Cytiva Life Sciences, CAT#, 17548115, column volume = 4.7mL, resin size-exclusion = 700kDa, max protein load = 13 mg ovalbumin/mL resin ). Following column installation, the entire system was flushed with 3-5 CV of 18.2Ω double-filtered MilliQ at 2mL/min. To clean the system, a double-filtered solution of 0.5N BioUltra NaOH, 30% isopropyl alcohol (Decon Labs CiDehol70, CAT# 8401) in 18.2Ω double-filtered MilliQ was flushed through the system at 0.5mL/ min for 1 hour to ensure the column is free of binding contaminants. Following cleaning the entire system was flushed of 18.2Ω double-filtered MilliQ at 2mL/min and then equilibrated with double-filtered D-PBS (Gibco, CAT# 14190250) for 3-5CV until the UV280 absorbance was stable, the absorbance was autozero set and then monitored for another CV until stable. Once the system was equilibrated the sample syringe was connected to the sample line and the sample was injected at 1mL/min. The UV280 absorbance was monitored for the duration of the injection until the absorbance value of passing particles began to plateau indicating column saturation of sample wherein fractions were collected using the Frac30 (Cytiva Life Sciences, CAT# 29023051) at 12mL per fraction until the entire sample was injected and the absorbance value dropped to the equilibrated value. Fractions collected were pooled in a 50mL centrifugal tube (Corning, CAT# 430290) and concentrated using Amicon Ultra-15 Centrifugal filters Ultracel-10 K (Millipore, Cat# UFC901024) briefly, the centrifugal filters were pre-equilibrated with double-filtered D-PBS at 4000xg for 10 minutes. The retentate and flow through were discarded and the FPLC-EV sample was added to the tube and

concentrated to a final volume of 8-12mL by spinning the sample down at 4000xg for 10 minutes at room temp until the desired volume was achieved. The concentrated EV sample was collected in a 20mL syringe (BD Bioscience) and sterile filtered with a 0.2 μm Acrodisc 25 mm syringe filter (Pall Life Sciences, Cat# 4612) into a new sterile 15mL tube (Corning, CAT# 430053) to be used for functional assessment and characterization.

**ISEV Characterization: Nanoparticle tracking analysis (NTA) of EVs using the NanoSight NS300:**

EVs were analyzed by nanoparticle tracking analysis (NTA) using the NanoSight NS300 (Malvern Panalytical). A hundred microliters of EV-rich sample were used for NTA and diluted 1:10 in double-filtered D-PBS to a final volume of 1 mL of EV sample for analysis. Each sample was vortexed prior to filling the syringe with the sample and the syringe pump from Harvard Apparatus (CAT. # 98-4730) was used for acquisition in flow mode. Each 1-mL sample was run using the following script: six captures of 1 min at speed 10 on flow mode. For capture settings, a camera level of 15 was used for all samples and a detection threshold of 30 was used for analysis resulting in approximately 30 particles per frame. Analysis of the raw data was performed using the NTA 3.0 software (Malvern Panalytical) where analysis of five out of six captures was performed, removing the first capture to generate the approximate total EV concentration. Following NTA data analysis using the NTA 3.0 software, Excel was used to account for the dilution factor 10.

**ISEV Characterization: Immunophenotyping of EVs using the MACSplex Exosome kit of 37 specific markers:**

The MACSplex Exosome kit (human) (Miltenyi Biotec, CAT# 130-108-813), (i.e., multiplex bead-based flow cytometric analysis) was conducted as per the manufacture's recommendations for the "Overnight protocol for the assay using 1.5 mL reagent tubes" with modifications outlined below. EVs isolated by PEG precipitation or TFF +FPLC were assessed using the MACSplex Exosome kit where 460 µL of EV sample were transferred to 1.5-mL Protein LoBind tubes (Eppendorf, CAT.#0030.108.116) where 40 µL of MACSplex Exosomes Capture Beads was added to each EV sample and incubated overnight. Detection of EVs was done using the CD63/ CD81/CD9 MACSplex Exosome Detection Reagent cocktail. Following labeling, samples were transferred to 5-mL FACS tubes (BD Biosciences, CAT# 382058) and analyzed by flow cytometry using the FACSAria Fusion flow cytometer (BD Biosciences). Ten thousand events per sample were collected. Raw data was analyzed using FlowJo V10 (FlowJo LLC, USA). For data processing, buffer-only control for each specific bead was used for background subtraction for the respective bead population. Following buffer subtraction, the IgG isotype control signal was subtracted from all bead populations. Finally, the detection threshold was set based on the residual signal present in the negative channels.

**Protein Specific Immunoprecipitation of EVs for Surface Marker Identification:**

Target specific isolation of EVs was done using antibody-conjugated magnetic bead precipitation for specific proteins to confirm surface presentation of potential identity markers of hBM-MSC-

EVs. The Dynabead Antibody Coupling kit (Invitrogen, CAT# 14311D) was used as per manufactures recommendation to conjugate the following antibodies for EV assessment; anti-human NRP1 (Novus Biological, CAT# DDX0440P-100) anti-human CD63 (Novus Biological, CAT# NBP2-42225) and mouse IgG1 (Novus Biological, CAT# NBP2-62028). Briefly, the entire vial of 60mg of M-270 epoxy Dynabeads was washed with C1 solution, wherein the beads were prepped and conjugated to each antibody at a concentration of 5ug of antibody/mg of beads to a final volume of 6000uL. The antibody bead mixture was incubated overnight on a thermomixer at 1200RMP at 37°C to ensuring the beads did not settle in the tube. The conjugated beads were then washed with BD, LB, and SB solution and resuspended at a final concentration of 10mg/mL.

**Protein Isolation and Quantification by Bicinchoninic Acid (BCA) 562nm Assay:**

To assess the quantity of NRP1 present in the EVs, 250µL of isolated EVs were mixed with a 5X stock of RIPA Buffer (Alfa Aesar, CAT# J62524-AE) containing HALT Protease/ Phosphatase Inhibitor (ThermoFisher, CAT# 78441) to a dilution of 1X and incubated for 45 minutes to lyse the EVs for protein isolation. Protein lysates were then spin down at 14,000 X g for 5 minutes to pellet insoluble proteins, and the protein suspension was transferred to a low protein binding tube for storage at -80°C freezer. Determination of protein concentration of EV lysates was done using the Pierce BCA Protein Assay kit (ThermoFisher Scientific, Cat# 23225) as per manufactures recommendations for plate-based assessment. EV protein lysates were tested at 1:2 dilution as well as undiluted in triplicates. The standard curve used for concentration interpolation was assessed using linear regression ($R > 0.990$).

**Quantification of NRP1 by Intact and Lysed EVs:**

To assess the quantity of NRP1 present in the EVs, 50µL of EV lysate or intact EVs were tested using the Quantikine Human Neurpilin-1 ELISA kit (R&D Systems, Cat# DNRP10) as per manufactures recommendation. Briefly, EV samples or standard curves were incubated in coated plates for 2 hours at room temperature on a plate shaker at 500rpm. Wells were washed with 400µL of Wash Buffer and then incubated with anti-Neuropilin-1 conjugate for 2 hours. The wells were washed again with 400µL of wash buffer before being incubated with Substrate solution for 30 minutes, before being quenched and read on the Biotek EpochMX plate reader at 450nm, 520nm, and 560nm. Background correction of absorbance and plate distortion was done using 520 and 560nm correction. Concentrations were extrapolated for unknown samples using 4-PL non-linear regression (R>0.990) Graphpad prism Version 7.0.

**Quantitative Proteomic Analysis of hBM-MSC EVs for Molecular Profiling:**

**Sample Cleanup and Fractionation:**

Samples were thawed on ice and desalted using the spin columns supplied in the EasyPep™ Mini MS Sample Prep Kit (ThermoFisher, product A40006) according to the manufacturer's directions, dried in a vacuum centrifuge, and re-suspended in 100 µL 0.1% FA. Peptide amount was determined using a Quantitative Colorimetric Peptide Assay (Pierce, 23275). Equal amounts of each labeled digest were combined and diluted with water to 900 µL and fractionated into 8 fractions (fraction-1 through fraction-8) with High pH Reversed-Phase Peptide Fractionation Kit (Pierce, 84868) according to the manufacturer's directions for TMT-labelled peptides. Fractions

were evaporated to dryness and resuspended in 20 µL injection buffer (0.1% formic acid in water) prior to LC-MS/MS analysis.

**Mass Spectrometric analysis:**

Samples were analyzed with an Orbitrap Fusion Lumos Mass Spectrometer coupled to an Easy-nLC 1200 (ThermoFisher Scientific) which was calibrated by infusion prior to analysis with a mixture of caffeine, MRFA, and Ultramark 1621. For LC-MS/MS, each fraction was analyzed in triplicate, 1-2 µL were loaded onto a NanoViper Acclaim pepmap 100 trap column (75 µm 20 mm with 3 µm beads) and desalting with 0.1% formic acid in water (solvent A) before separating on an Easyspray pepmap C18 reverse-phase analytical column (75 µm 500 mm with 2 µm beads). Chromatographic separation was achieved at a flow rate of 0.300 µL/min over 140 min in five linear steps as follows (solvent B was 0.1% formic acid in 80% acetonitrile): initial, 5% B; 80 min, 25% B; 120 min, 40% B; 130 min, 95% B; 140 min, 95% B. The eluting peptides were analyzed in data-dependent mode MSMS. An MS survey scan of 400−1400 m/z was performed in the Orbitrap at 120000 resolution, a 50 ms maximum injection time, and an AGC target of 4×105. The top speed mode (3 seconds) was used to select ions for MS2 analysis with dynamic exclusion of 20 seconds with a ± 10 ppm window. During the MS2 analyses, precursors were isolated using a width of 0.7 m/z and fragmented by HCD with collision energy 35%, followed by Orbitrap analysis at m/z 110-1000 at 50000 resolution, a 120 ms maximum injection time, and an AGC target of 1×105.

**Data Processing:**

The software package Proteome Discoverer 2.4 (ThermoFisher) was used to process the data. The SequestHT search engine was used to search MS2 spectra against a human protein database

(Trembl, downloaded 20200703, 54506 entries) and a database containing common laboratory contaminants (cRAP, downloaded 20180509, 116 entries) with MS1 / MS2 tolerances of 10ppm/. Fixed modifications were carbamidomethylation (+57.02146 Da) of cysteine residues, TMTpro (+304.207 Da) on lysine, and peptide N-terminal. Variable modifications were oxidation (+15.995 Da) of methionine, protein N-terminal acetylationMet-loss / -131.040 Da (M), Met-loss+Acetyl / -89.030 Da (M).

For quantification, Reporter Integration was Most Confident Centroid with tolerance 20 ppm, quantifying on Unique + Razor peptides, co-isolation tolerance 50%, and average reporter S/N threshold 7, Normalization none, scaling none.

**Peripheral Blood Mononuclear Cell (PBMC) Immunomodulatory Assessment: Assessment of Frozen Peripheral Blood Mononuclear Cells (PBMCs) for Cell Proliferation Tracking Using Lipid Dye:**

Pre-screened frozen PBMCs from healthy individuals were obtained commercially from Stem Cell Technologies under material transfer agreement and stored in liquid nitrogen until ready for processing. To determine the ideal culture conditions for stimulatory proliferation assessment. PBMCs were thawed as per manufactures recommendation using RPMI1640 with Glutamax (Gibco, CAT# 61870-036) containing 1M of HEPES (Gibco, CAT# 156300-80), 10% Heat inactivated FBS (Gibco, CAT# 12484028), and 30U/mL of recombinant human IL-2 (Gibco, CAT# PHC0026) (i.e. RPMI-C). PBMC suspension was transferred to a 15mL centrifuge tube and then spun down at 1200rpm for 10 minutes and the supernatant was discarded, and the pellet was

re-suspended in1mL D-PBS containing 5% heat-inactivated FBS (CFSE Solution). One microliter of Cell Trace CFSE (Invitrogen, CAT# C34554) was added to the cell suspension and incubated for 5 minutes at room temperature. Ten milliliters of CFSE solution were added to the cell suspension and spun down at 1200rpm for 10 minutes at room temperature to wash residual dye. The washing process was repeated 2 additional times. Following the dyeing process, cells were re-suspended in RPMI-C media and counted using Trypan Blue Assessment. The cells were then plated in black-walled tissue culture treated flat bottom 96 well plate (Corning, CAT# 3595) at 100,000 cells per well. For proliferation assessment, CD3/28 Dynabeads were washed as per the manufacture's recommendations and the stimulatory controls were added at ratios of 1:1, 1:3, or 1:5 (beads: cell). Stimulation was allowed to proceed for 4 days wherein matched replicates (5-6 wells) were pooled in 5mL FACS tubes (BD Biosciences, CAT# 382058) and analyzed for proliferation assessment on the FACSAria Fusion (BD Bioscience), 50,000 events were collected, and data analysis was done using FlowJo Version 10.7.

**Immunophenotyping of PBMC for Immune Cell Subtype Profiling:**

Following aseptic thaw of PBMCs (Stem Cell Technologies, CAT# 70025.1, Lot# 2003), 500,000 cells were transferred to two 5mL FACS tubes for 12 colour multiplex fluorescent antibodies staining for the following surface cell markers: CD3-PerCP-Cy5.5 (eBiosciences, CAT# 45-0036-41), CD4-APC (BD Bioscience, CAT# 561840), CD8-BV421 (BD Bioscience, CAT# 562428), CD14-PE-Cy7 (BD Bioscience, CAT# 560919, CD16-BUV737 (BD Bioscience, CAT# 564433), CD19-PE-CF594 (BD Bioscience, CAT#562321), CD25-BV786 (BD Bioscience, CAT# 563701), CD40-BV510 (BD Bioscience, CAT# 563456), CD45-FITC (BD Bioscience, CAT# 560976),

CD69-BV650 (BD Bioscience, CAT# 563835), HLA-DR-APCFire750 (BioLegend, CAT# L23105) and UV450 dead cell stain. Briefly, the tubes were spun down at 1200rpm for 8 minutes and re-suspended in 500uL of flow buffer (D-PBS+ 2% FBS). For stained sample containing antibody master mix or the unstained control containing PBS was incubated for 30 minutes at 4°C, where it was then washed once using 1mL of flow buffer and spun down at 1200rpm for 8 minutes. Following the spin, the supernatant was aspirated, and cells were re-suspended in 500µL of flow buffer for flow analysis on the FACSAria Fusion. 100,000 gated events were collected. Compensation for each fluorophore was set up using 1 drop of negative and positive compensation beads (BD Bioscience) with each antibody in a separate tube. Flow results were analyzed using FlowJo (Version 10).

**Assessment of hBM-MSCs or hBM-MSC-EVs for Immunomodulatory Potency using Frozen PBMCs Proliferation Assay.**

Pre-screened frozen PBMCs from healthy individuals were obtained commercially from Stem Cell Technologies under material transfer agreement and stored in liquid nitrogen until ready for processing. To determine the ideal culture conditions for stimulatory proliferation assessment. PBMCs were thawed as per manufactures recommendation using RPMI1640 with Glutamax (Gibco, CAT# 61870-036) containing 1M of HEPES (Gibco, CAT# 156300-80), 10% Heat inactivated FBS (Gibco, CAT# 12484028), and 30U/mL of recombinant human IL-2 (Gibco, CAT# PHC0026) (i.e. RPMI-C). PBMC suspension was transferred to a 15mL centrifuge tube and then spun down at 1200rpm for 10 minutes and the supernatant was discarded, and the pellet was re-suspended in1mL D-PBS containing 5% heat-inactivated FBS ( i.e. CFSE Solution). One

microliter of Cell Trace CFSE (Invitrogen, CAT# C34554) was added to the cell suspension and incubated for 5 minutes at room temperature. Ten millilitres of CFSE solution was added to the cell suspension and spun down at 1200rpm for 10 minutes at room temperature to remove the residual dye. The washing process was repeated 2 additional times. Following the dying process, cells were re-suspended in RPMI-C media and counted using Trypan Blue Assessment. The cells were then plated in black-walled tissue culture treated flat bottom 96 well plate (Corning, CAT#) at 100,000 cells per well. For proliferation assessment, CD3/28 Dynabeads (Invitrogen, CAT# 11131D) were washed as per manufactures recommendations and the stimulatory controls were added at a ratio of 1:3 (beads: cell). Either 30,000 hBM-MSCs or hBM-MSC-EVs at a concentration of (0.25-1.25X10^9 particles/ well) were added to stimulated samples to address immunomodulatory effects. Stimulation was allowed to proceed for 4 days wherein matched replicates (5-6 wells) were pooled in 5mL FACS tubes (BD Bioscience, CAT# 352058) and analyzed for proliferation assessment on the FACSAria Fusion (BD Bioscience), 50,000 events were collected, and data analysis was done using FlowJo Version 10.7.

**Statistical Analysis of Experimental Data in GraphPad Prism:**

Where applicable, statistical analysis for significance testing was conducted on experimental replicates to assess the probability of a true result. Min-Max value normalization was completed on data where the minimum and maximum values were obtained by experimental controls to linearize the value distribution for analysis. Statistical analysis was completed in Graphpad Prism version 7.0, where; $p<0.05$ = *, $p < 0.01$ = **, $p <0.001$ = *** and $p < 0.0001$ = **** using one way - analysis of variance (ANOVA) with Tukey's post hoc test as well as Tukey's multiple

comparison test were used to analyze differences between experimental samples (Tukey, "Comparing Individual Means in the Analysis of Variance", 1949, Biometrics).

## Chapter 4: Results

### hBM-MSC Thaw and Expansion:

The human BM-MSCs were obtained from (RoosterBio Inc.) at a passage number of 0-1. Cells were pre-characterized by the company for ISCT established criteria of CD105+, CD90+, CD73+, CD45- and HLA-DR- surface receptor population and differentiation into the trilineage (chondrocytes, osteocytes, and adipocytes). To obtain enough cells to seed the hollow fiber cell bioreactor was expanded under 2D culture using the CS10 stack flasks. The *in vitro* expansion potential of the cells was examined based on the observed population doubling time (Figure 1). Including the recovery phase following liquid nitrogen thaw, all hBM-MSC cell lines exhibited a doubling time of less than 48hours (2 days) consistent with the originating population doubling criteria obtained from the manufacturer**.** Additionally, the cumulative population doubling of the hBM-MSCs was calculated to determine the overall cell population's age as MSCs have a limited *in-vitro* age range where they are in their prime functional condition and an exhausted MSC population may affect the EV characterization. All donors used in EV production remained under 10 cumulative population doublings following expansion (Figure 1) and were considered in their peak culture range as per the RoosterBio recommendations.

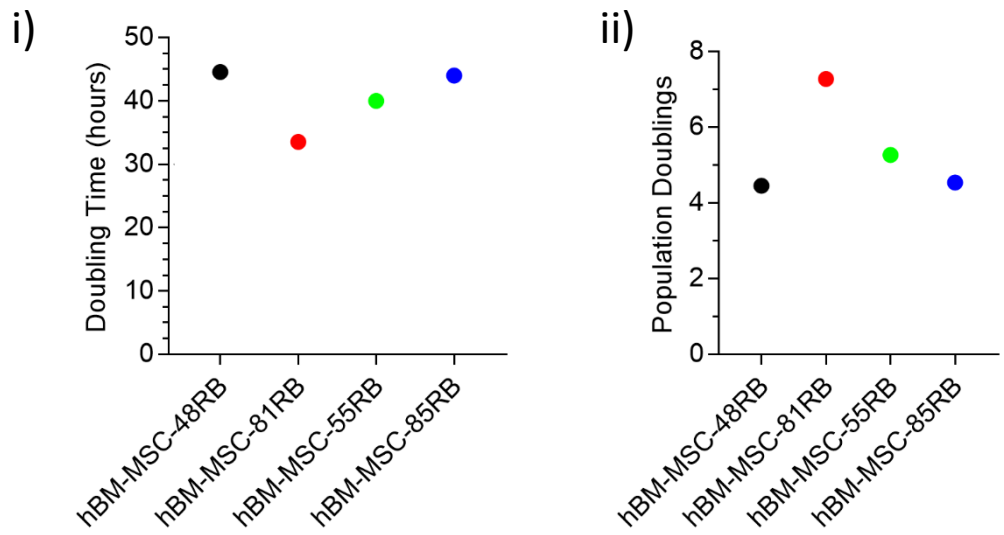


**Figure 1: Characterization of hBM-MSC culture age confirmed cells expanded for EV production were within the functional age range.** Each donor was expanded before hollow fiber cell bioreactor inoculation to increase inoculation density and assess the pre-bioreactor proliferation characteristics of the MSCs. Assessment of growth characteristics was done by trypan blue dye exclusion cell counting to determine the number of viable cells. I) The interpolated population doubling time of each MSC donor was calculated based on a 5-day expansion including the recovery phase from frozen. Doubling times were calculated based on Roth V. 2006 methodology. II) Cumulative population doubling was calculated as per (Ahsan & Adlerz, RoosterBio 2019) to confirm each hBM-MSCs donor is being used within a similar expansion range. Counts were conducted on (Invitrogen Countess II) in duplicates with a 20% coefficient of variance (CoV) accepted. Samples with greater than 25% CoV underwent additional counts to reduce variability.

**Hollow Fiber Bioreactor MSC Culture: Metabolic Characterization**

Following inoculation of the hBM-MSC into the hollow fiber cell bioreactor, the overall health of the cell population was determined by measurement of the main observable metabolites (Figure 2) glucose and lactic acid. As recommended by FiberCell Systems, ideal maintenance of the cellular population in the bioreactor for biological production would indicate consistent glucose consumption with equivalent or less lactic acid production as waste byproducts. The glucose concentration of the media was measured before inoculation to obtain a baseline assessment of the glucose content and then every 2-3 days to ensure glucose consumption remained consistent during EV production. During the initial inoculation phase (Day 0-3) glucose consumption was at a rate higher than 0.2g/L/day then the glucose consumption reduced following the transition to EV collection medium to less than 0.2g/L/day for the duration of the EV production. Lactic acid measurement was done to assess metabolic stress through EV production. The lactic acid concentration increased during the initial inoculation phase (Day 0-3) and appeared to decrease during the interim EV production phase where it remained below 0.1g/L for the duration of EV production.

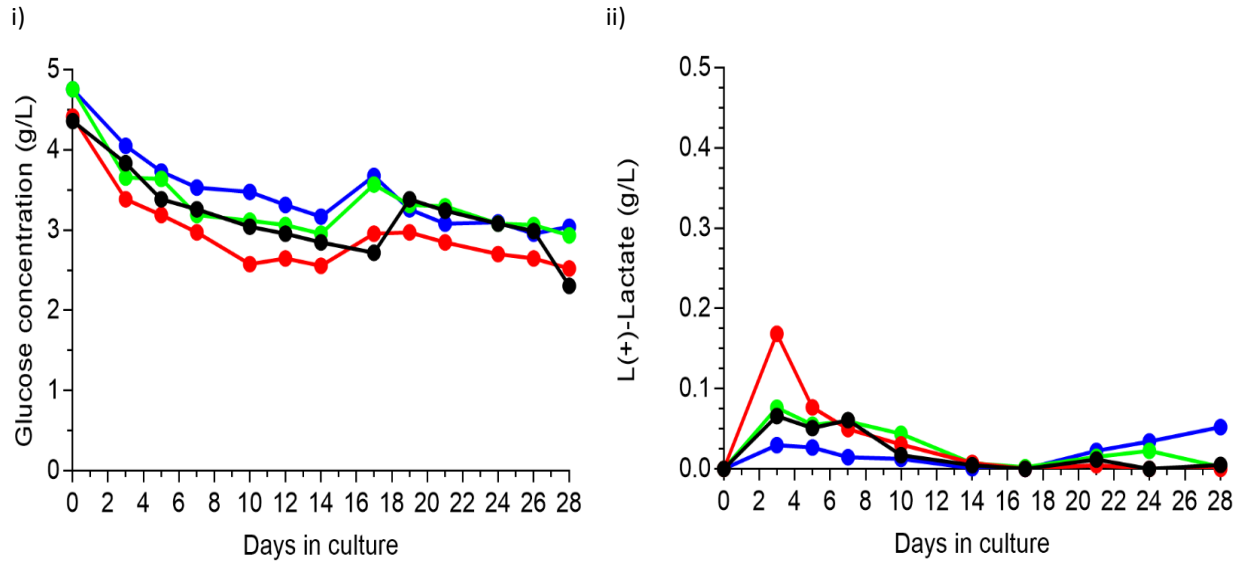

**Figure 2: Metabolite analysis of hBM-MSCs during serum-free bioreactor EV production showed consistent glucose consumption with minimal lactic acid production.** To determine to the overall health of the cells in the closed-loop hollow fiber cell bioreactor, each EV production run was monitored for glucose and lactic acid cellular metabolites on alternating media sample harvests. I) Conditioned media glucose content was monitored using the AccuCheck Model 930 to determine the glucose consumption of the cells during EV production and indicate the 50% glucose cutoff for media replenishment. II) Lactic acid was measured in the media samples by colorimetric assay to assess if cells were metabolically stressed during EV production. Glucose measurements were done in singlets. Lactic acid measurements were done with 2 technical replicates.

**ISCT MSC Characterization:**

Each hBM-MSC donor was characterized as per the ISCT guidelines before and after EV production. Cells maintained the MSC surface profile (Figure 3A) consisting of greater than 99% expression of CD105+, CD90+, and CD73+, as well as less than 0.1% expression of negative markers CD34-,CD11b-,CD19-, CD45- and HLA-DR- population. Cells were able to differentiate into the trilineage (chondrocytes, osteocytes, and adipocytes) (Figure 5). Cells were confirmed to adhere to plastic after being cultured in flasks for expansion before inoculation.

Following EV production in the bioreactor system. Cells were harvested and characterized following the same ISCT guidelines to reaffirm MSC identity. Greater than 95% of cells exhibited expression of CD90 and CD73 but showed reduced expression (less than 5% positive expression) of CD105 after 25 days of culture in a bioreactor media system **(**Figure 3B). Additionally, post

bioreactor cells also incurred low (less than 15% positive) negative marker expression (Figure 4). This was addressed by investigating which protein was being expressed from the negative marker cocktail (CD34, CD11b, CD19, CD45, or HLA-DR). We confirmed through single marker staining the negative marker observed from the cocktail was CD34 (Appendix A1) To elucidate the low CD105 expression as well as the increased expression of CD34 following extended bioreactor culture, bioreactor harvested cells were returned to normal serum media conditions (RoosterBio MSC complete media) for 7 days in 2D flask culture. All hBM-MSC donors observed full recovery of (greater than 99% positive) CD105 expression (Figure 4) and were able to differentiate into the trilineage (chondrocytes, osteocytes, and adipocytes) (Figure 5). Negative markers were also reassessed and expression returned to normal (Less than 0.1% positive) following 2D culture recovery (Figure 4). These results concluded no permanent changes to MSC morphology following 25 days of EV bioreactor production.

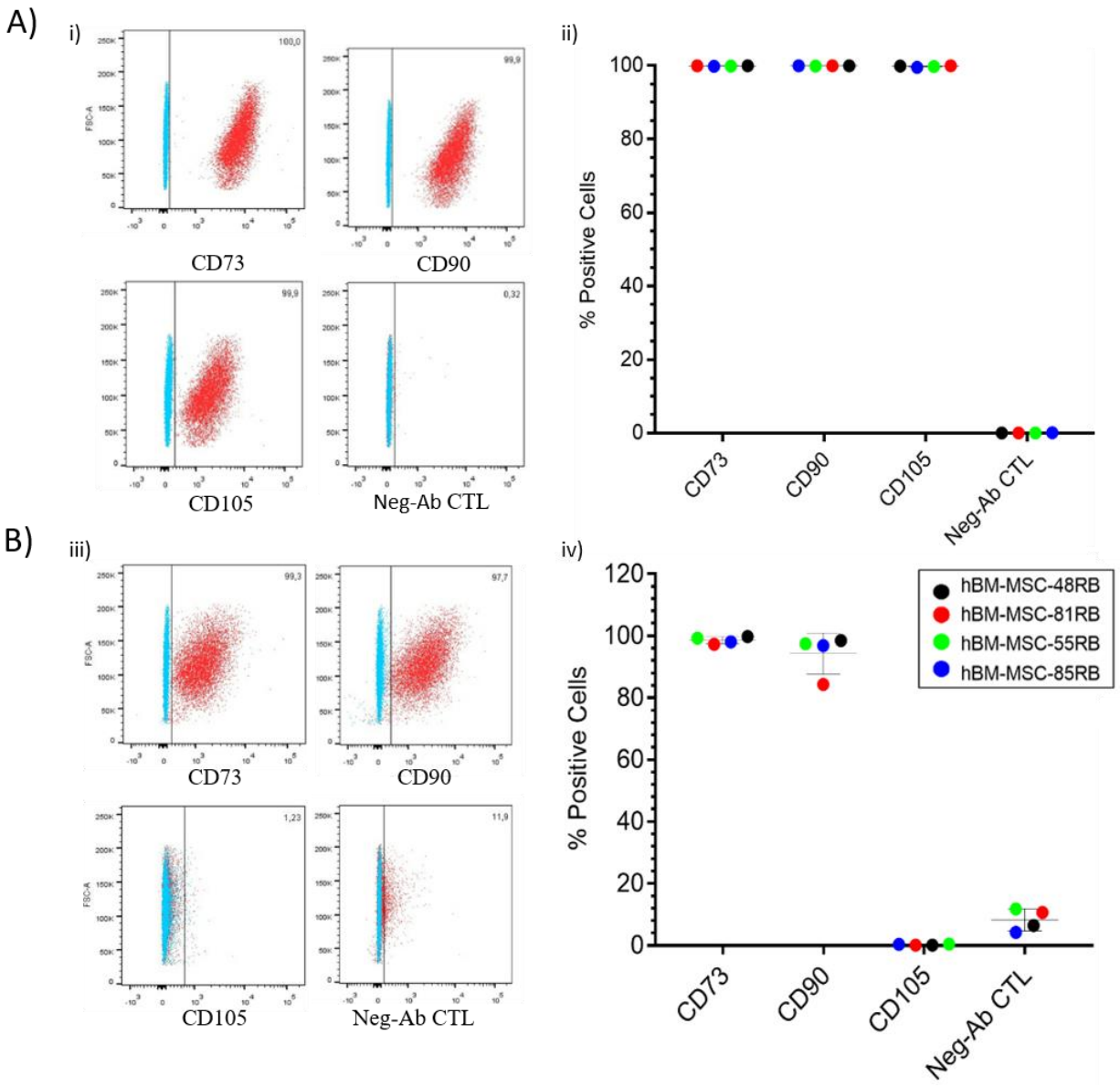


**Figure 3: hBM-MSC ISCT Characterization of MSCs during serum-free bioreactor EV production confirms maintenance of the majority of MSC-associated markers.** A) Flow cytometric analysis of MSC surface profile to confirm MSC identity before bioreactor exposure. I) Dot plot of hBM-MSC-55RB as a representation of flow analysis where the Blue population is isotype control and Red population is the representative MSC Staining. Cells were individually stained for MSC established markers CD73 (APC) CD90 (FTIC) CD105 (PerCP-Cy5.5) and

Negative antibody cocktail control (PE) II) Quantitative representation of immunophenotyping of surface markers for each donor for the percentage of positive parent staining. B) Flow cytometric analysis of MSC surface profile to confirm MSC identity following 25 days of EV production. III) Dot plot of hBM-MSC-55RB as a representation of flow analysis where the Blue population is isotype control and Red population is the representative MSC Staining. Cells were individually stained for MSC established markers CD73 (APC) CD90 (FTIC) CD105 (PerCP-Cy5.5) and Negative antibody cocktail control (PE) IV) Quantitative representation of immunophenotyping of surface markers for each donor for the percentage of positive parent staining. Flow cytometry analysis was conducted on the BD Bioscience FACSAria Fusion, data collection was done using FACSDiva, and post-collection analysis was done using FlowJo Version 10.7. Samples were analyzed in duplicate with fluorophore compensation.

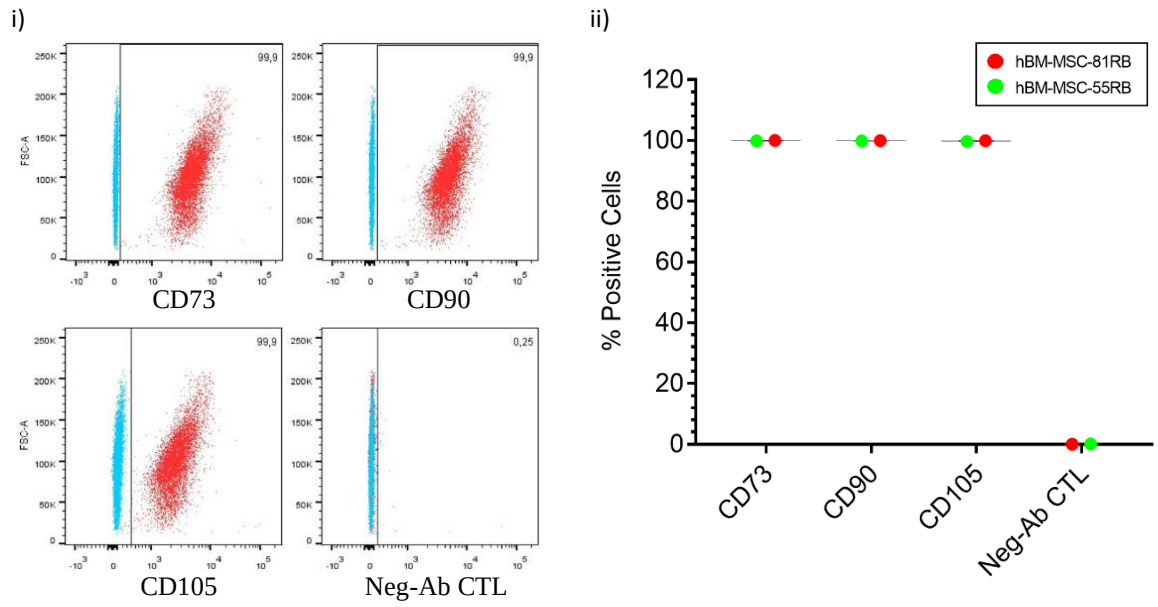


**Figure 4: hBM-MSC ISCT flow cytometry characterization of MSCs recovered post EV production returned to traditional serum 2D culture showed full MSC marker identity.** Flow cytometric analysis of MSC surface profile to confirm MSC identity following 25 days of EV production. I) Dot plot of hBM-MSC-55RB as a representation of flow analysis where the Blue population is isotype control and Red population is the representative MSC Staining. Cells were individually stained for MSC established markers CD73 (APC) CD90 (FTIC) CD105 (PerCP-Cy5.5) and Negative antibody cocktail control (PE) II) Quantitative representation of immunophenotyping of surface markers for each donor for the percentage of positive parent staining. Flow cytometry analysis was conducted on the BD Bioscience FACSAria Fusion, data collection was done using FACSDiva, and post-collection analysis was done using FlowJo Version 10.7. Samples were analyzed in duplicate with fluorophore compensation.

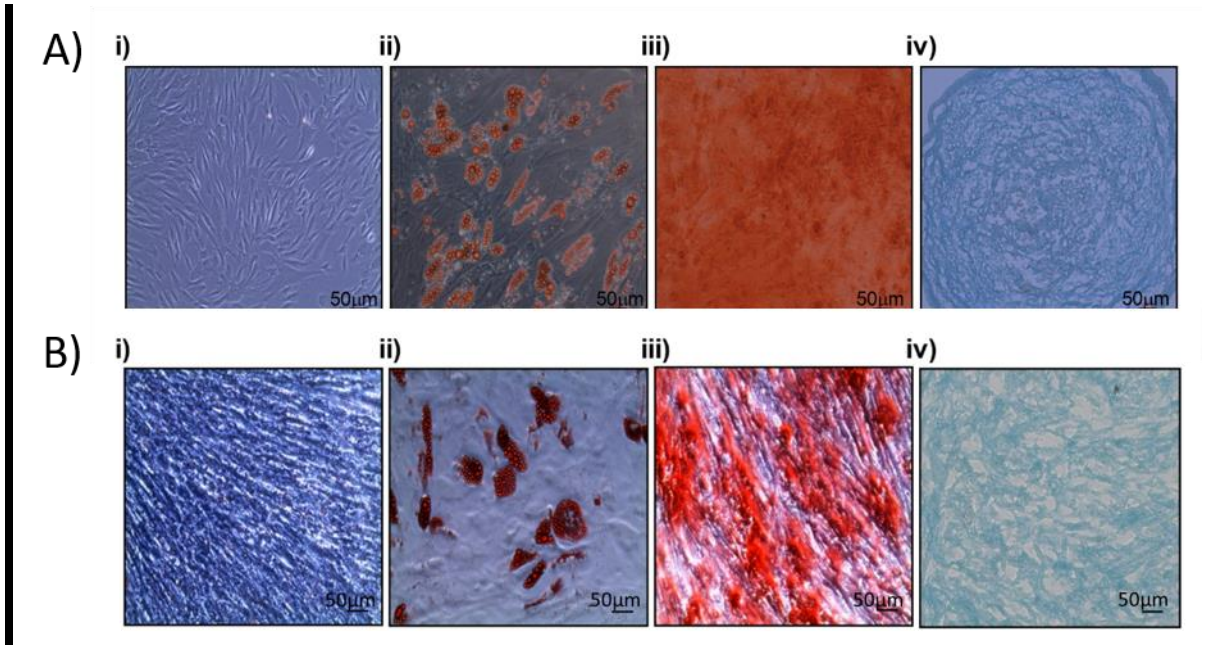


**Figure 5: ISCT characterization of hBM-MSCs for trilineage differentiation potential throughout bioreactor EV production confirmed MSC maintained their progenitor function.** **A)** Differentiation assessment was done on hBM-MSC expanded for bioreactor production. Cells were differentiated as per StemXVivo differentiation protocol for Adipocytes, Osteocytes, and Chondrocytes. I) hBM-MSC cultured in normal RoosterBio MSC media representative of undifferentiated control. II) hBM-MSCs cultured for adipocyte differentiation, stain with Oil Red O to indicate Adipocyte cells. III) hBM-MSCs cultured for osteocyte differentiation, stain with Alizarin S to indicate calcium deposits indicative of osteocyte cells. IV) hBM-MSCs cultured for chondrocyte differentiation, stain with Alcian Blue 8GX to indicate the collagen matrixed of chondrocyte cells. B) Differentiation assessment was done on hBM-MSC retrieved from bioreactor following EV production. Cells were differentiated as per StemXVivo differentiation protocol for Adipocytes, Osteocytes, and Chondrocytes. I) hBM-MSC cultured in normal RoosterBio MSC media representative of undifferentiated control. II) hBM-

MSCs cultured for adipocyte differentiation, stain with Oil Red O to indicate Adipocyte cells. III) hBM-MSCs cultured for osteocyte differentiation, stain with Alizarin S to indicate calcium deposits indicative of osteocyte cells. IV) hBM-MSCs cultured for chondrocyte differentiation, stain with Alcian Blue 8GX to indicate the collagen matrixed of chondrocyte cells. Differentiation was completed in 24 well plates with 3 technical replicates. The microscopic assessment was completed using Zeiss Observer II at 10x objective.

**ISEV Size Characterization Time Point Analysis:**

Following the ISEV 2018 guidelines, hBM-MSC-EVs from all four donors were characterized for respect to size distribution, surface profile, and proteomics profile. All donors were tested at three different time points associated with each day of harvest (days 1-2 (start), days 13-14 (interim), and days 24-25 (end)). Nanoparticle tracking analysis of the hBM-MSC-EVs isolated from three different time points over 25 days of hollow fiber bioreactor EV production showed consistent EV production concerning the size distribution of particles over time (Figure 6A). All donors contained particles less than 205nm for its most abundant populations.

Statistically, hBM-MSC-EVs isolated from all 4 donors regardless of time point confirm the average mean and mode particle sizes (Figure 6B) remained under 200nm in diameter. Quantile statistical analysis of the nanoparticle tracking analysis confirmed at the $10^{th}$, $50^{th,}$ and 90th percentile interval represented the coefficient of variance for the size distribution observed to have a size distribution of particles less than 205nm, except for donors hBM-MSC-EV-48RB and 81RB which observed particle range less than 225nm (Appendix A2) There was observable variability

between concentrations of selective samples between times points, however, this cannot be confirmed without reassessment of several independent bioreactor production trials.

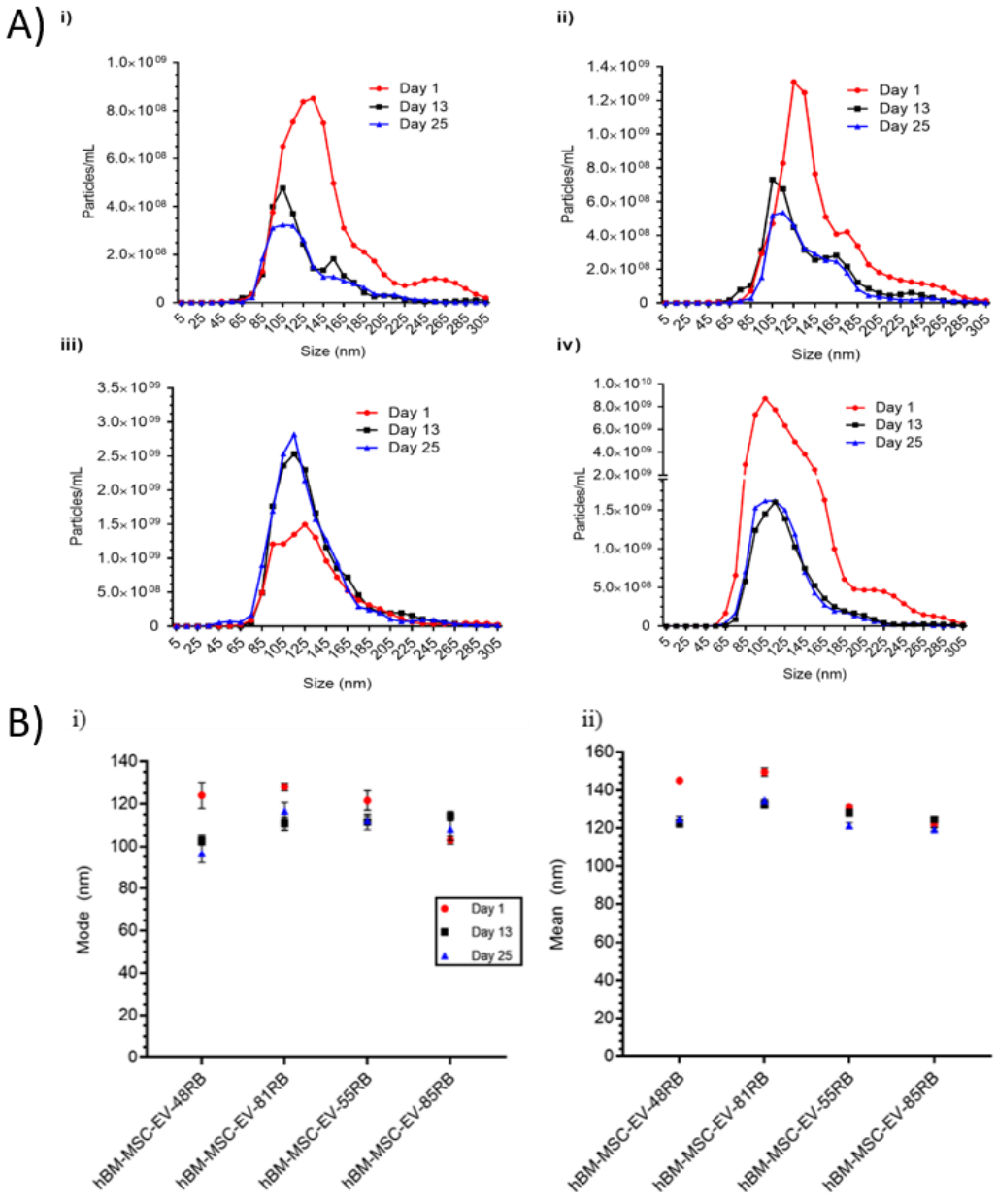


**Figure 6: Nanoparticle Tracking Analysis of hBM-MSC-EV analyzed at different time points of production to assess size distribution confirmed small EV profile. A)** Nanoparticle tracking

analysis of isolated EV produced from hBM-MSCs in the hollow-fiber cell bioreactor system assessed for ISEV size distribution of total particles. Histogram plots of nanoparticle size concentration and distribution of the four hBM-MSC donors; I) hBM-MSC-48RB, II) hBM-MSC-81RB, III) hBM-MSC-55RB, and IV) hMB-MSC-85RB at three different time points (days 1, 3, and 25) of EV production. Red represents EV sample isolated from day 1, black represents EV sample isolated from day 13, and blue represents the EV sample isolated from day 25. B) Averaged mean and mode values from NTA analysis analyzed from main population size. I) Nanoparticle tracking analysis comparing the average mode EV size of each production time point for all 4 donors. II) Nanoparticle tracking analysis comparing the average mean EV size of each production time point for all 4 donors. Red represents EV sample isolated from day 1, black represents EV sample isolated from day 13, and blue represents the EV sample isolated from day 25. Analysis was completed NanoSight NS300 (Malvern Panalytical) on flow mode each dot represents the average concentration of particles for a binned size (5 technical replicates).

**ISEV Surface Marker Profiling: Time Point Analysis**

Characterization of intact particles to confirm the identity of hBM-MSC-EVs was validated for their surface profile by a multiplex bead-based flow cytometry analysis. EV-associated markers were confirmed for tetraspanins CD63, CD81, and CD9 as well as MSC-associated markers CD105, CD44, CD146, and CD29 (Figure 7) confirm MSC-EV identity**.** Variability was observed in the relative abundance of the identification markers between days but the variability was not consistent with a pattern associated with a specific time point. Additionally, all donors observed negligible identification of immunoreactivity HLA proteins. Additional markers such as CD49e,

CD20, CD56, MCSP, ROR1 SSEA-4, CD41B, and CD142 were observed in lower abundance and at varying levels but consistently between donors and time points.

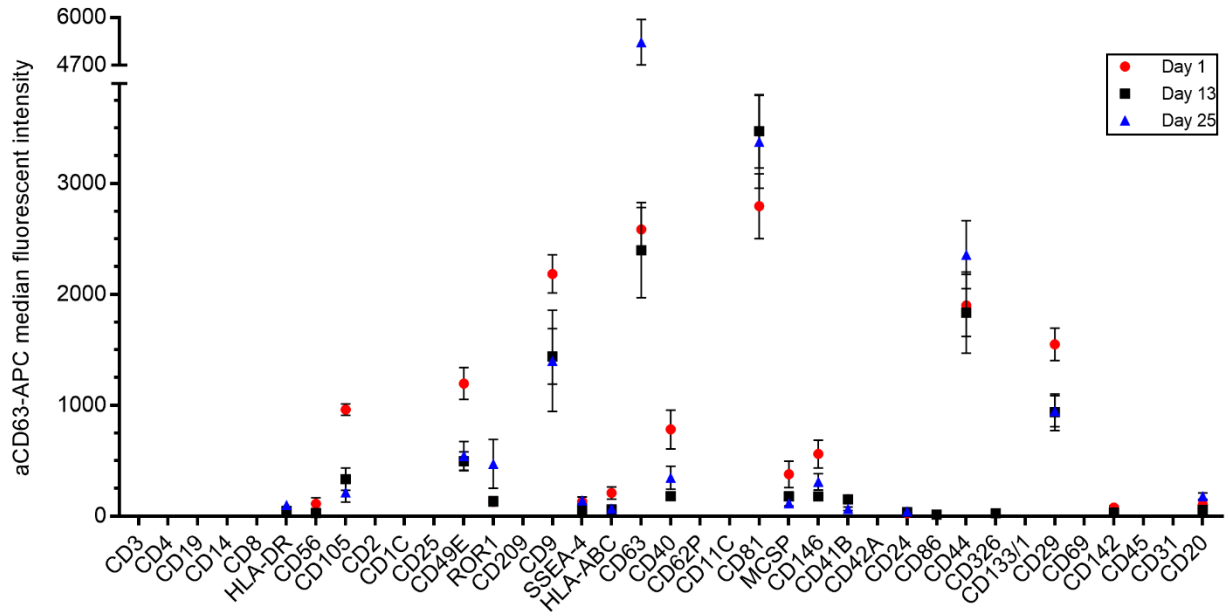


**Figure 7: Flow cytometric characterization of the hBM-MSC-EV surface profile during different time points of EV production.** Quantitative assessment of 37 distinct surface proteins expression compared between three different time points of production of 4 hBM-MSC-EV donors 48/81/55/85RB, respectively. Each sample was stained with CD63/CD81/CD9 APC antibody cocktail to identify the EV-bead population and determine marker abundance. Flow cytometry analysis was conducted on the BD Bioscience FACSAria Fusion, data collection was done using FACSDiva, and post-collection analysis was done using FlowJo Version 10.7. Samples were analyzed in duplicate with fluorophore compensation. Each EV donor and time point sample were analyzed with three experimental replicates.

**ISEV Protein Characterization for EV Identity Validation: Time**

**Point Analysis**

Categorization of the isolated particles obtained from the hBM-MSC bioreactor production as EVs was confirmed by protein identification of EV-associated proteins following the ISEV established EV protein categories. Proteomics analysis was repeated for each donor and time point to validate the established protein molecules as per the ISEV 2018 guidelines as indicated in **(Table 1)** at least one of each protein was identified for the representative categories in all donors and at all analyzed time points (Data Not Shown). Additionally, previously determined MSC-EV markers were confirmed (CD44, CD105) including NRP1 which was previously determined to be associated with hBM-MSC-EVs.

**Table 1: Proteomics Analysis Validates ISEV Criteria of all Bioreactor produced hBM-MSC-EVs:** Proteomics was conducted on protein lysates produced from hBM-MSC-EV isolates from all 4 donors and three different time points. Peptide abundance was calculated using TMT labeling counts. As per the ISEV guidelines EVs were required to observe at least one protein of categories 1, 2, and 3 must be identified to show EV origin and the level of purity of an EV preparation. Category 4 is supported the identification of proteins associated with small EVs, and category 5 was assessed for functional molecules). Additionally, category 6 was included to identify markers shared from the parental cell of origin to support MSC-EV identity.

| **Category 1** | **Category 2** | **Category 3** | **Category 4** | **Category 5** | **Category 6** |
|---|---|---|---|---|---|
| | | | | | |

| Transmembrane / GPI-anchored proteins related to the plasma membrane or endosome | Cytosolic proteins present in EVs | Additional non EV structures proteins | Transmembrane and soluble proteins related to other intracellular compartments | Secreted proteins present with EVs | Cell of origin associated protein markers |
|---|---|---|---|---|---|
| **CD63, CD81, CD9** | **TSG101** | **APOA2** | **HSPA8** | **VEFG-A** | **CD44, NRP1, CD105** |

**Surface Marker Profiling: NRP1 validation:**

Previously established MSC-EV identity marker NRP1 was validated for MSC-EV surface presentation by magnetic immunoprecipitation of hBM-MSC-EVs following isolation of EVs from hBM-MSC-175RB ECM produced by the hollow fiber bioreactor. Following IP, the EVs were tested for NRP1 abundance by ELISA to determine the prevalence of NRP1 presenting EVs (Figure 8). The Control group using the established CD63 marker showed antibody capture protocol was able to pull down EVs based on surface presentation. NRP1 specific beads were used to isolate NRP1 presenting EVs from EV isolate directly to assess frequency. An isolated MSC-EV stock sample was used to compare the pulldown efficiency compared to a direct EV sample. The MSC-EV stock observed a higher abundance value of NRP1 indicated more EVs present in the stock sample compared to the pulled-down isolates at the same test volume. The pulled-down samples showed comparable abundance values when isolated using CD63 or NRP1.

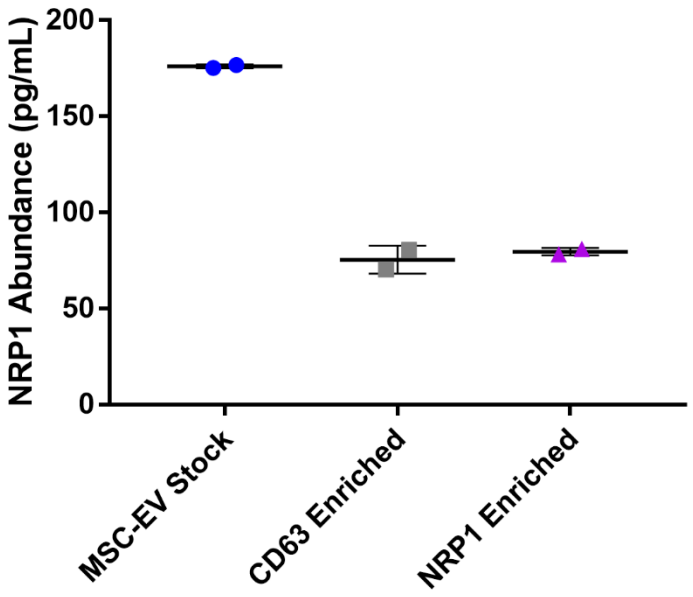


**Figure 8: Assessment of Surface Presenting NRP1 abundance for each hBM-MSC-sEV donor.** Surface presentation of NRP1 was determined by intact EV immunoprecipitation (IP) of target-specific antibody-conjugated magnetic beads to identify of hBM-MSC-EVs NRP1 frequency in the heterogeneous EV population. Isolated EV samples from hBM-MSC-EV donor 175RB, were co-incubated with either CD63 conjugated magnetic beads (CD63 enriched), NRP1 conjugated magnetic beads (NRP1 enriched), or no beads (MSC-EV stock). EVs bound to beads were removed by the magnet and all samples were extracted by trituration and analyzed by NRP1 ELISA.

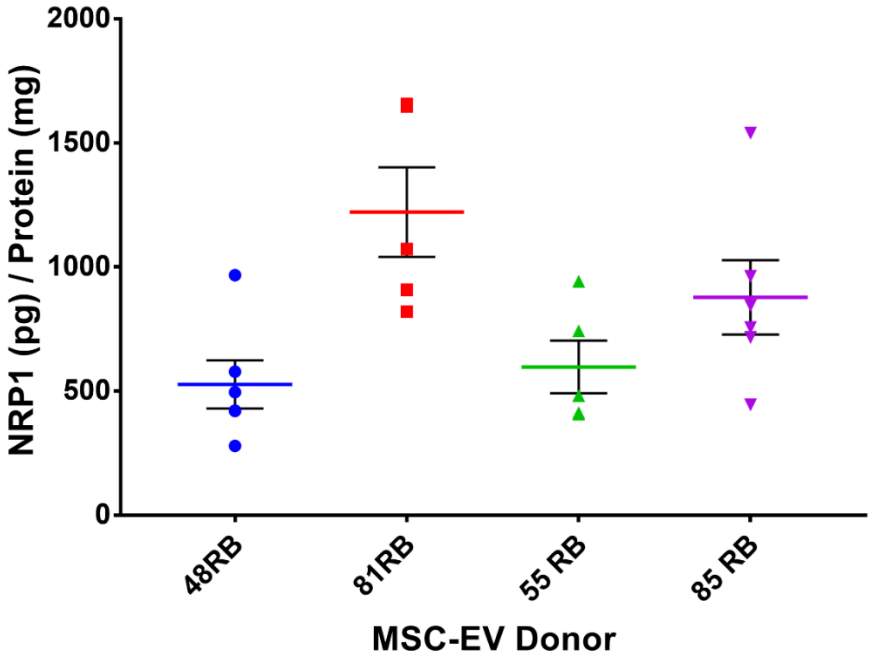


**Figure 9: Assessment of NRP1 abundance for each hBM-MSC-sEV Compared to Overall EV Protein Abundance.** As a potential marker for identifying hBM-MSC-EVs, NRP1 was assessed for EV lysates by ELISA to determine the abundance of NRP1 for each donor per milligram of EV protein. Isolated EV sample from each hBM-MSC-EV donor; 48/81/55/85RB, respectively, where lysed protein content was determined by BCA. Lysed EV protein was then assayed, with (N=2), independent experiments with 6 technical replicates included in each experiment.

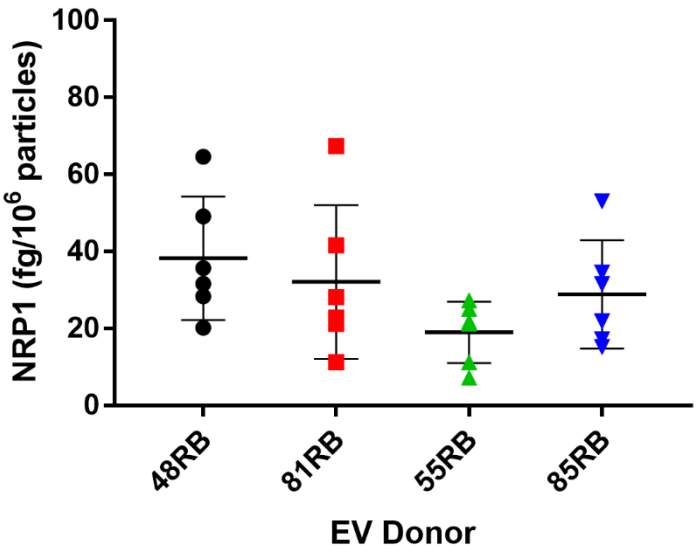


**Figure 10: Assessment of NRP1 Abundance for each hBM-MSC-sEV donor per One Million Particles.** Further investigation of hBM-MSC-EVs and NRP1 was done to determine the abundance of NRP1 for each donor per EV particle. Isolated EV sample from each hBM-MSC-EV donor; 48/81/55/85RB, respectively, where lysed protein content was determined by BCA. Lysed EV protein was then assayed, with (N=2), independent experiments with 6 technical replicates included in each experiment. NRP1 abundance per particle was determined using the estimated particle concentration of the sample by nanoparticle tracking analysis to determine the total particle content per volume. The total particle content of each lysed sample was then normalized to the observed NRP1 abundance. Particle concentration was analyzed on NS300 using NTA3.0 software. Colorimeter analysis of protein content and NRP1 ELISA was measured on the Biotek Epoch MX at 562nm and 460nm/520nm, respectively.

**Particle profile of each hBM-MSC-EV donor analyzed by FPLC during EV Purification**

Scalable isolation of hollow fiber bioreactor-produced hBM-MSC ECM was implemented to improve the volume range of downstream applications using tangential flow filtration and fast protein liquid chromatography. Analysis of the ECM during FPLC purification observed the total content of the ECM during injection (Figure 11). As shown, each donor showed comparable concentrations of soluble material in the ECM after pre-filtering indicated by consistent UV280nm absorbance of ECM samples between 150 and 190 A280 for each donor once the FPLC column was saturated with the sample.

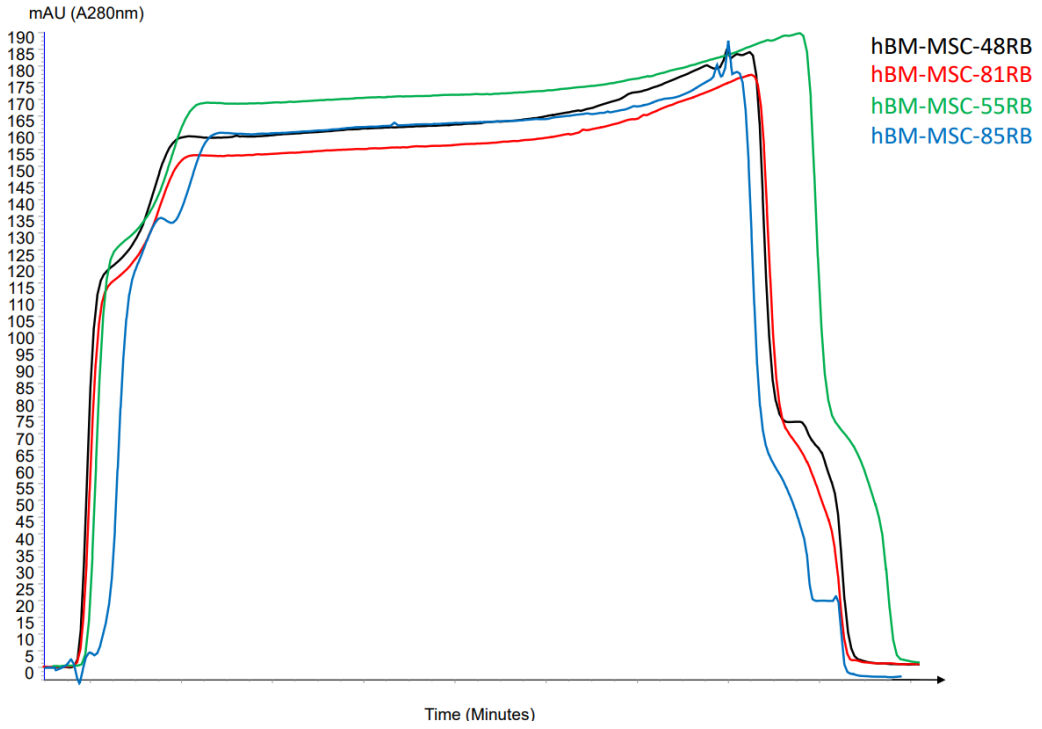


**Figure 11: Purification of tangential flow filtration pretreated hBM-MSC-sEV containing cell-conditioned media processed by HiScreen CaptoCore 700 multimodal affinity column.** Up to 50mL of TFF pre-cleared/pre-concentrated EV containing media (ECM) was injected into the FPLC containing the HiScreen CaptoCore 700 column for 700kDa size-exclusion protein

binding affinity purification. Following the initial injection of the sample, fractionation was started once the UV A280nm absorbance indicated the column was saturated representative by a UV A280nm signal plateau. 15mL fractions were collected over time until the UV A280nm signal dropped indicated the sample injection was complete. Post column clean in place protocol was done to assess the amount of contaminant bound during the cleaning procedure. Purification was completed on the AKTAStart FPLC system (GE Life Science).

**Nanoparticle Tracking Analysis: Scalable Isolation Analysis**

Furthermore, following recovery of scaled EV sample isolated from the TFF+ FPLC workflow, Samples were re-characterized for size distribution and particle concentration estimation by nanoparticle tracking analysis to reaffirm the ISEV suggested size attributed of EVs. Each bioreactor-produced hBM-MSC donor ECM was re-characterized for frequency of size and distribution (Figure 12). The size range and profile of particles isolated following TFF and FPLC were nearly identical comparing each hBM-MSC-EV donor observed to have a consistent size distribution with the majority of particles less than 205nm, however, both hBM-MSC-48RB and 81RB were less concentrated than hBM-MSC- 55RB and 85RB following isolation of the same volume of starting ECM. The mean and mode of each donor were re-assessed and observed to share an average particle size of less than 200nm (Figure 13). Finally, quartile distribution of expected particles at the $10^{th}$, $50^{th,}$ and 90th percentile intervals were completed (Appendix A3). Each hBM-MSC-EV donor was observed to have an average size distribution of particles less than 200nm.

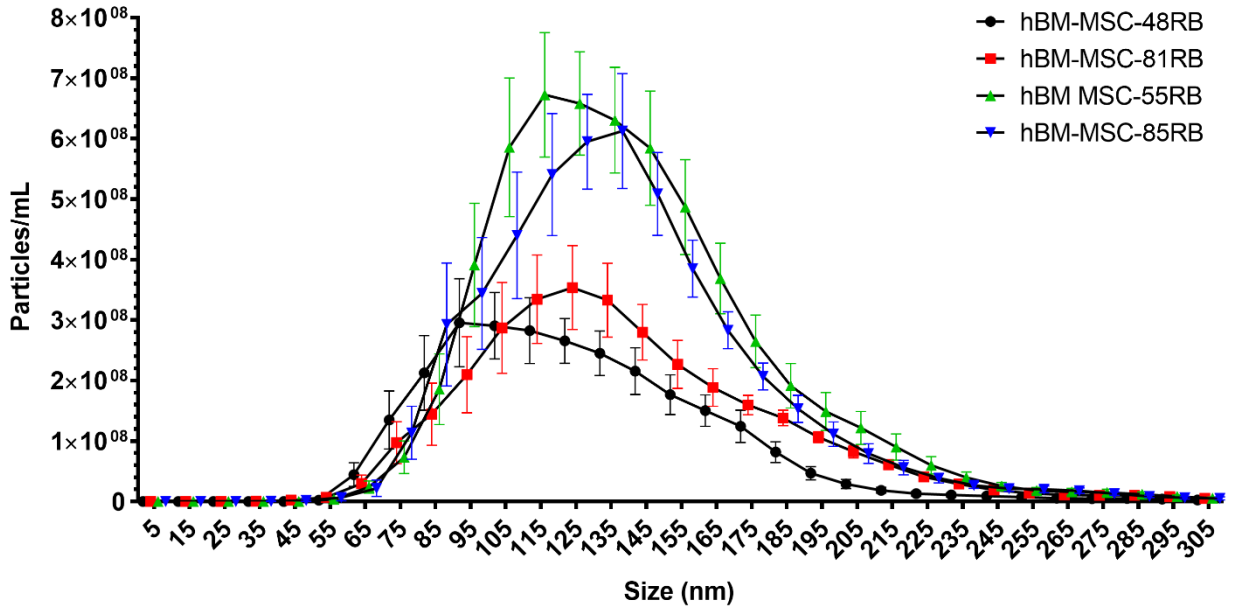


**Figure 12: Nanoparticle Tracking Analysis of TFF+FPLC purified hBM-MSC-sEV to assess size distribution.** Nanoparticle tracking analysis of TFF+FPLC isolated EV produced from hBM-MSCs in the hollow-fiber cell bioreactor system for EV characterization analysis to determine to the size distribution of the purified particles per the ISEV 2018 guidelines. EVs were analyzed on the NS300 (Malvern) using NTA 3.0 Software. N=3

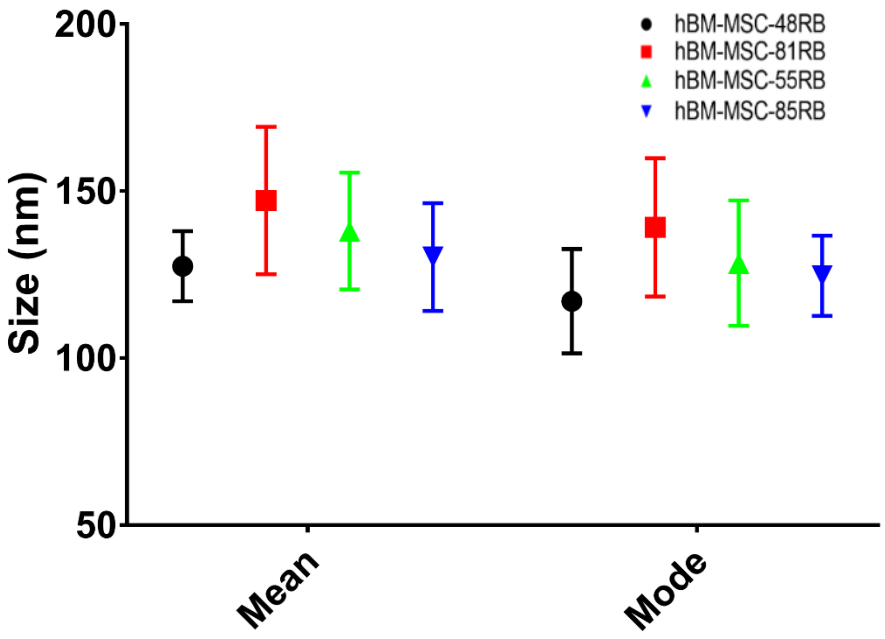


**Figure 13: Assessment of Mean and Mode particle size for hBM-MSC-sEV following FPLC Purification.** Each hBM-MSC-sEV sample was investigated for the mean and mode particle size to validate the particle size of the isolated EVs adheres to the small EV category of the ISEV2018 guidelines. EVs were analyzed on the NS300 (Malvern) using NTA 3.0 Software. N=3

**Nanoparticle Tracking Analysis: Scalable Isolation Hollow Fibre Bioreactor Theoretical hBM-MSC-EV Yield:**

Additional analysis was conducted on the nanoparticle tracking results to estimate the theoretical yield of the total number of particles produced and retrieved from the bioreactor with scalable TFF + FPLC EV (Figure 14). Total yields were projected based on isolation yields normalized to the volume of unprocessed starting ECM. Estimated yield of purified particles in the concentration of $10^{11}$ purified EVs total per bioreactor production with an average purified concentration of $10^{8}$ particles per mL of hollow fiber bioreactor produced hBM-MSC ECM.

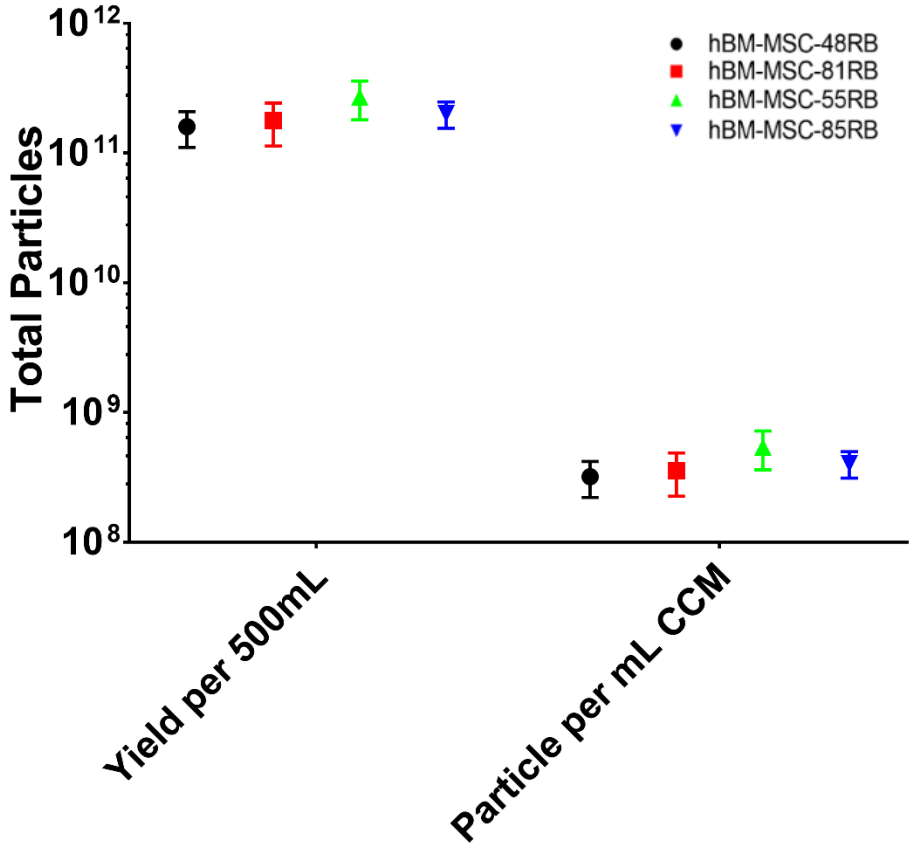

**Figure 14: Determination of small EV yield following bioreactor production and TFF+FPLC Purification.** The theoretical yield was calculated based on the estimated concentration determined by nanoparticle tracking analysis. Total yield per isolation was estimated then normalized to the volume of starting EV containing media (ECM). Each donor showed comparable yield per volume of ECM as well as for the total yield per bioreactor production. EVs were analyzed on the NS300 (Malvern) using NTA 3.0 Software. N=3

**ISEV Surface Marker Profiling: Scalable Isolation Analysis**

The TFF+FPLC purified particles were re-characterized to confirm the identity of hBM-MSC-EVs and were validated for an EV surface profile by a multiplex bead-based flow cytometry for EV identification. EV-associated markers were re-confirmed for tetraspanins CD63, CD81, and CD9 as well as MSC-associated markers CD105, CD44, CD146, and CD29 (Figure 15) confirm MSC-EV identity**.** Additionally, all donors observed negligible identification of immunoreactivity HLA-DR proteins and variable low expression of HLA-ABC protein. Additional markers such as CD49e, CD56, MCSP, ROR1 SSEA-4, CD41B, and CD142 were observed at varying levels.

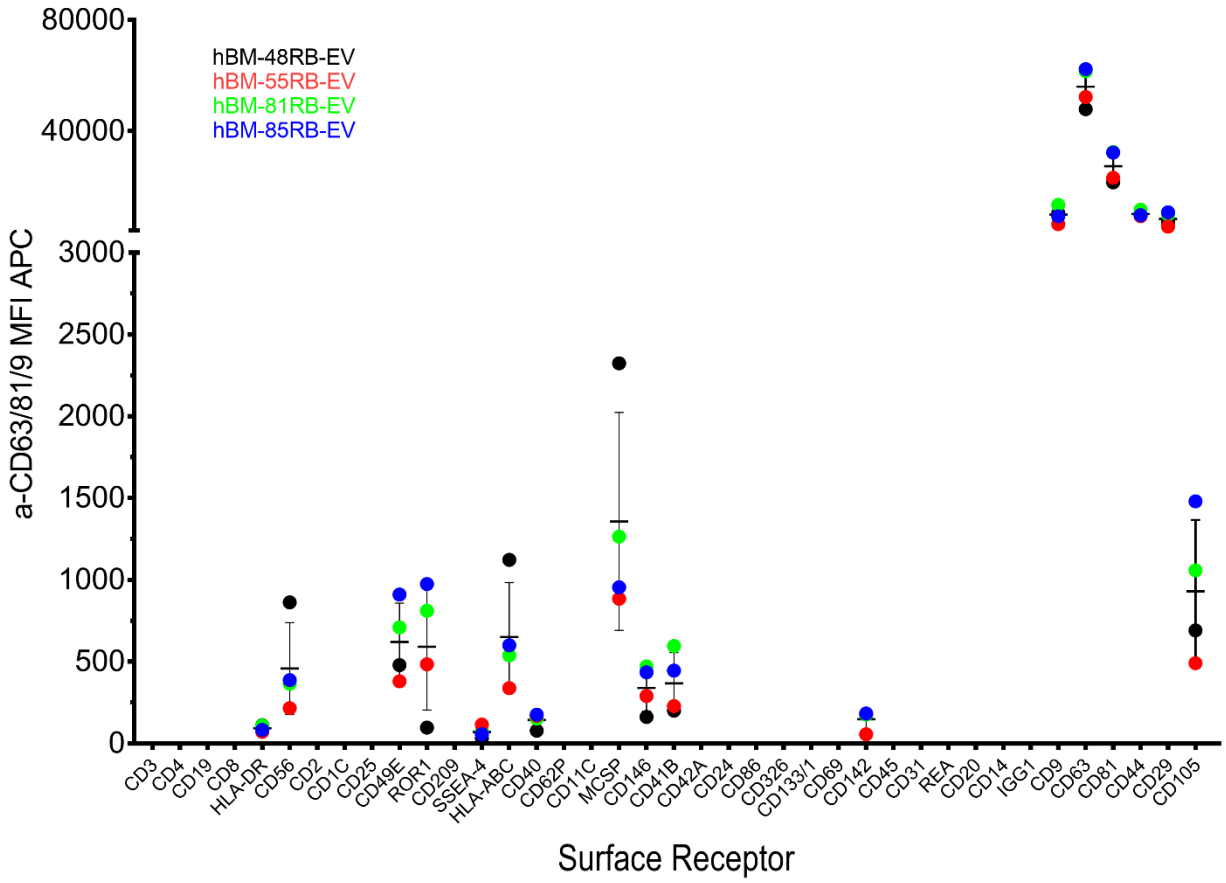


**Figure 15: Surface receptor assessment of 37 markers on small EVs isolated using TFF+FPLC purification.** Quantitative assessment of 37 distinct surface proteins expression compared between the production of 4 hBM-MSC-EV donors 48/81/55/85RB, respectively EV isolate from each donor processed using the TFF+FPLC purification scheme was analyzed for surface marker presentation of established EV associated markers as well as additional cell surface receptors for characterization of EV identity per the ISEV2018 guidelines. Each sample was stained with CD63/CD81/CD9 APC antibody cocktail to identify the EV-bead population and determine marker abundance. Flow cytometry analysis was conducted on the BD Bioscience FACSAria Fusion, data collection was done using FACSDiva, and post-collection analysis was done using FlowJo Version 10.7. Samples were analyzed in duplicate with fluorophore

compensation. Each EV donor and time point sample was analyzed with three experimental replicates. To emphasize time point analysis, the MFI of donor samples from the same time point were pooled for statistical analysis, and markers were analyzed for statistically significant changes between time points of production in Graphpad prism 7.0.

**Assessment of hBM-MSC-EV potency for immunoregulation of activated PBMCs.**

Evaluation of the function of hBM-MSC-EVs was done using an activated peripheral blood mononuclear cells to simulate an inflammatory environment *in vitro* like that of GvHD or other autoimmune or inflammatory diseases. The PBMC population was validated to assess the proportion of the heterogeneous immune cell population for different subtypes. (Figure 16) Flow cytometry assessment of the PBMCs by fluorescent multiplex immunostaining confirmed the presence of CD4+ and CD8+ T cells, as well as CD19+ B cells and a small proportion of natural killer cells when gating for lymphocyte populations. Additionally, the presence of monocytes (CD14+/CD16+), as well as dendritic cells (CD14+/HLA-DR+), was assessed (Figure 17). The CD14+/CD16+) monocytes represented up to 69% of the positive monocyte population compared to (CD14+/HLA-DR+) dendritic cells making up to 17% of the positive monocyte population. Conclusively, the identification of the main functional cell types of the mixed mononuclear cell population is complementary to an *in-vitro* immune cell model.

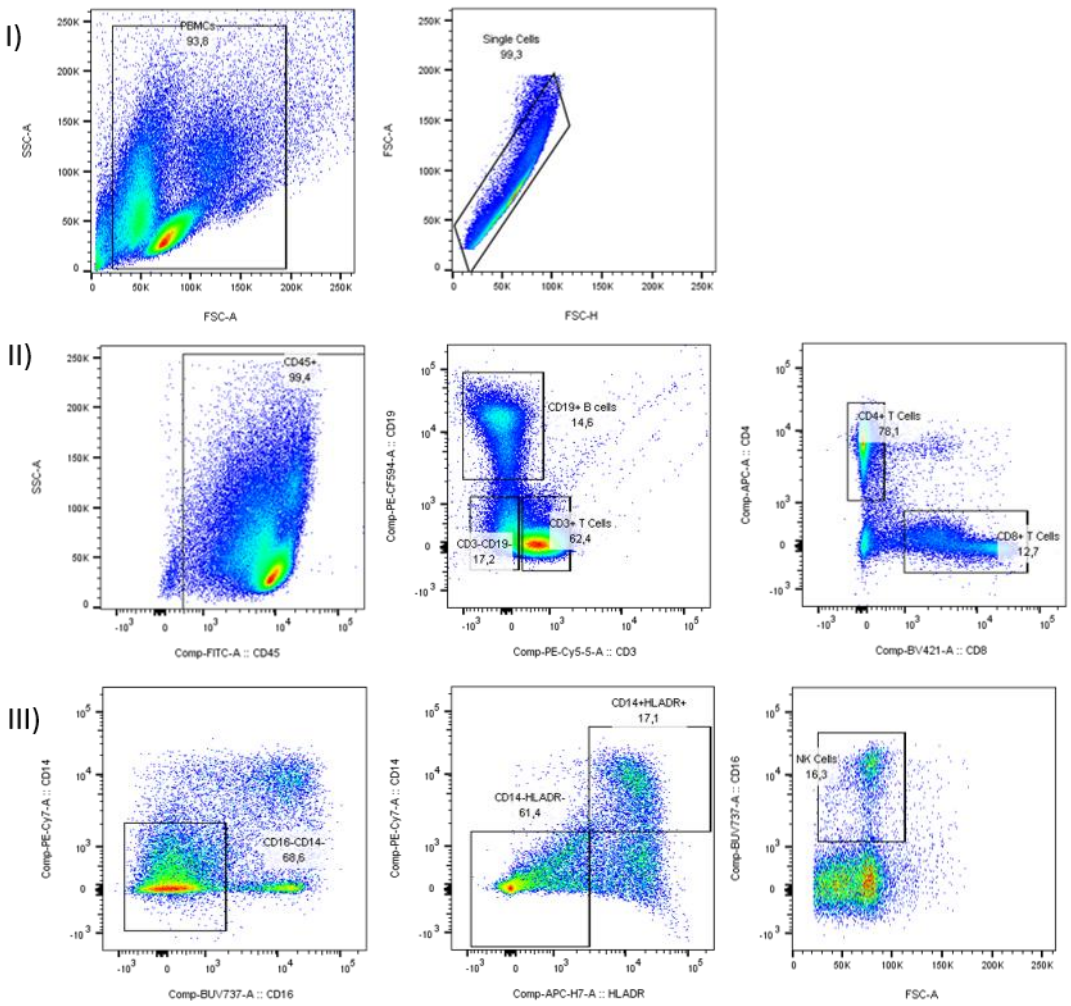


**Figure 16: Immunophenotype of lymphocyte population in peripheral blood mononuclear cell population used in proliferation assay by fluorescent multiplex flow cytometry.** Identification of individual immune cell subtypes was done on the PBMCs to map the population distribution. I) initial gating of PBMC population and single cell type analysis. II) CD45+ gating to assess the distribution of CD4+ and CD8+ T Lymphocytes as well as CD19+ B cells. III) CD45+ gating of CD16- NK Cells. Samples were run in duplicate with 100,000 events were collected on the FACSAria (BD Bioscience) using the FACSDiva software, and gating strategy was analyzed on FlowJo (Version 10).

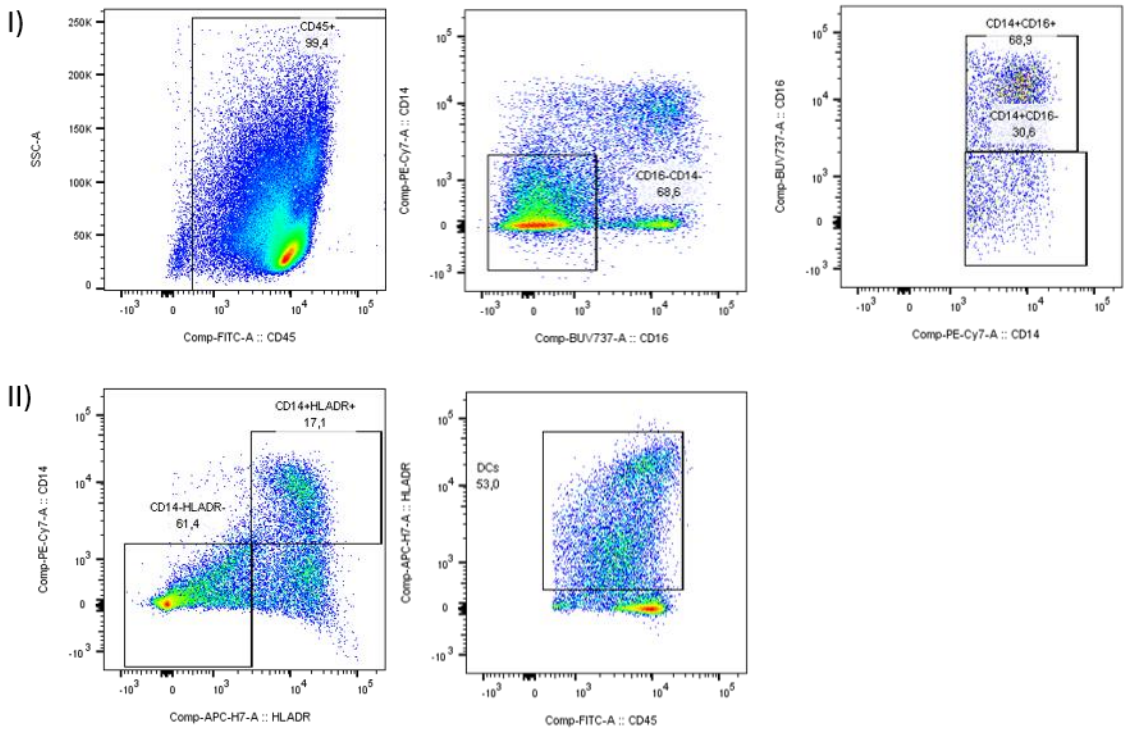


**Figure 17: Immunophenotype of monocyte populations in peripheral blood mononuclear cell population used in proliferation assay by fluorescent multiplex flow cytometry.** Identification of individual immune cell subtypes was done on the PBMCs to map the population distribution. I) Initial gating of CD45+PBMC population for CD14+ and CD16+ monocytes. II) CD14+ gating of HLADR+ expressing dendritic cells (DCs). Samples were run in duplicate with 100,000 events were collected on the FACSAria (BD Bioscience) using the FACSDiva software, and gating strategy was analyzed on FlowJo (Version 10).

**Functional Assessment of hBM-MSC-EVs: Dosing Analysis**

Characterization of the hBM-MSC-EV potency for immunomodulation was done by dose titration of single donor hBM-MSC-175RB (Figure 18). Additionally, testing the effect of particle concentration and dosing mechanism was measured through the assessment of multiple concentrations. Increasing concentration of hBM-MSC-sEV showed a slight improvement of suppression potential when considering a single dose (5000EVs/PBMC vs 12500EVs/PBMC, p-value<0.001) while multiple treatments at one lower dose did not seem to contribute significantly to improved effect at this scale (5000EVs/PBMC vs Multidose 5000EVs/PBMC).

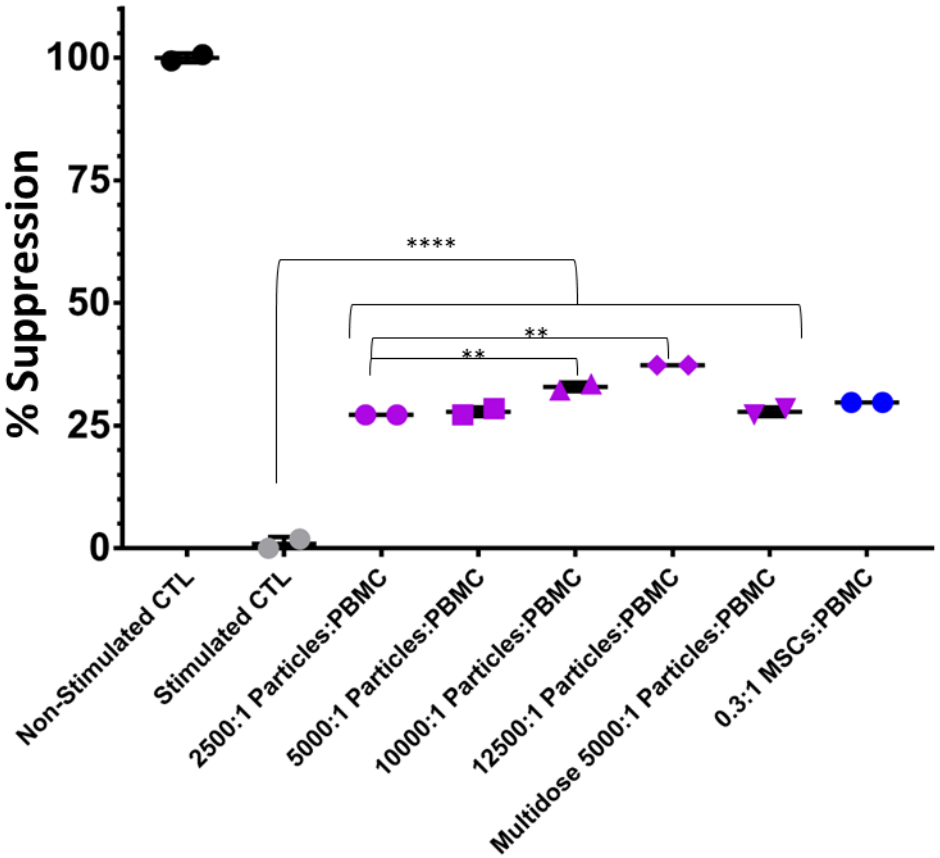


**Figure 18: Particle dosing assessment of hBM-MSC-sEV potency by PBMC proliferation assay.** Quantitative assessments of sEV derived from hBM-MSC-175RB were isolated using the TFF+FPLC workflow to determine the optimal particle dose per observable effect on

immunomodulation of the PBMCs. Single-dose titration was done as well as a multidose (treatment every 2 days). Results were obtained by CFSE proliferation dye assessment on the FACSAria (BD Bioscience) using the FACSDiva software, and the gating strategy was analyzed on FlowJo (Version 10). Percent suppression was calculated using min-max normalization of the CFSE expansion index for each sample compared to the non-stimulated (min) and stimulated (max) controls. Samples were incubated with MSCs or MSC-EVs for 4 days, N=2 with 1 technical replicate. Analysis conducted on Graphpad Prism version 7, one way ANOVA with Tukey's multiple comparison test where; $p<0.05$ = *, $p < 0.01$ = **, $p <0.001$ = *** and $p < 0.0001$ = **** using one way ANOVA and Tukey post hoc analysis.

**Functional Assessment of hBM-MSC-EVs: Donor to Donor Variability Analysis**

Determination of the functional donor-to-donor variability of the hBM-MSC-EVs was completed through an analysis of all 4 hBM-MSV-sEV donors (hBM-MSC-48RB/81RB/55RB/85RB) which were compared for function immunomodulation of the activated PBMC at the same concentration of 5000 particles/PBMC to observe the role of donor potency (Figure 19**).** When comparing the effect of cells to their respective EV treatments there is some variability in the results between donors but in all cases, each donor by cells or EVs showed considerable suppression potential of 30% or greater. (Figure 20) Donor to donor variability seems to be more apparent when comparing cells from different donors, where the variability of suppression when comparing EVs from different donors is less observable.

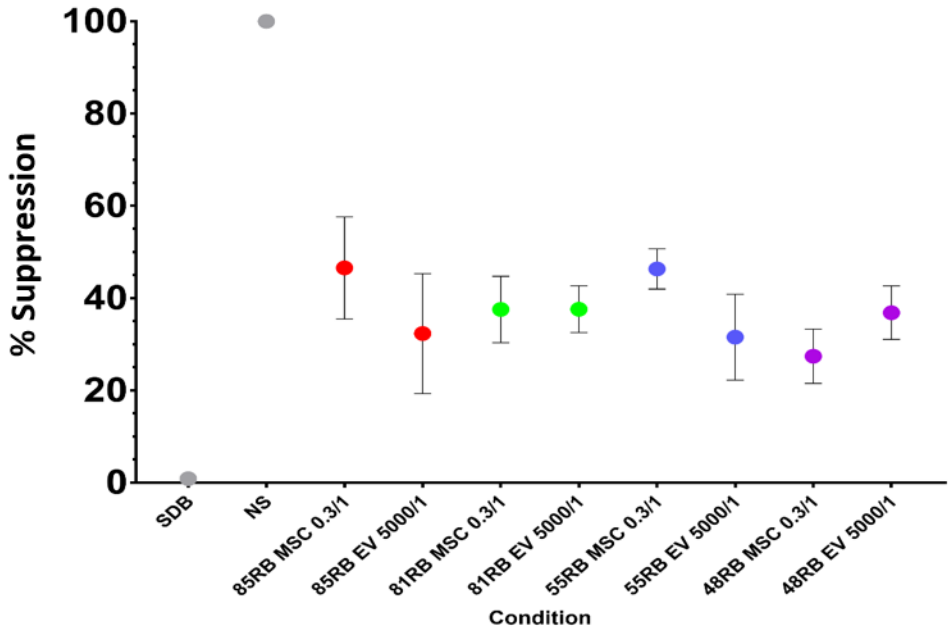


**Figure 19: Donor to donor potency of hBM-MSCs/sEV for immune suppression of activated PBMCs confirms functional effect.** hBM/MSCs or sEV from ECM derived from hBM-MSC-48RB/81RB/55RB/85RB were isolated using the TFF+FPLC workflow to address differences in sEV potency at a set dose by the observable effect on immunomodulation of the PBMCs. Each hBM-MSC/MSC-EV donor was tested at either 0.3 MSCs per 1PBMC or 5000 particles per 1 PBMC. Results were obtained by CFSE proliferation dye assessment on the FACSAria (BD Bioscience) using the FACSDiva software, and the gating strategy was analyzed on FlowJo (Version 10). Percent suppression was calculated using min-max normalization of the CFSE expansion index for each sample compared to the non-stimulated (min) and stimulated (max) controls. EV condition representative of all 4 hBM-MSC-sEV donor results combined. MSC condition representative of all 4 hBM-MSCs donor results. NS representative of the non-stimulated PBMC control. SDB condition representative of activated PBMC control with CD3/28 dynabeads to determine proliferation rate following stimulation. N=3, independent experiments with 2 technical replicates.

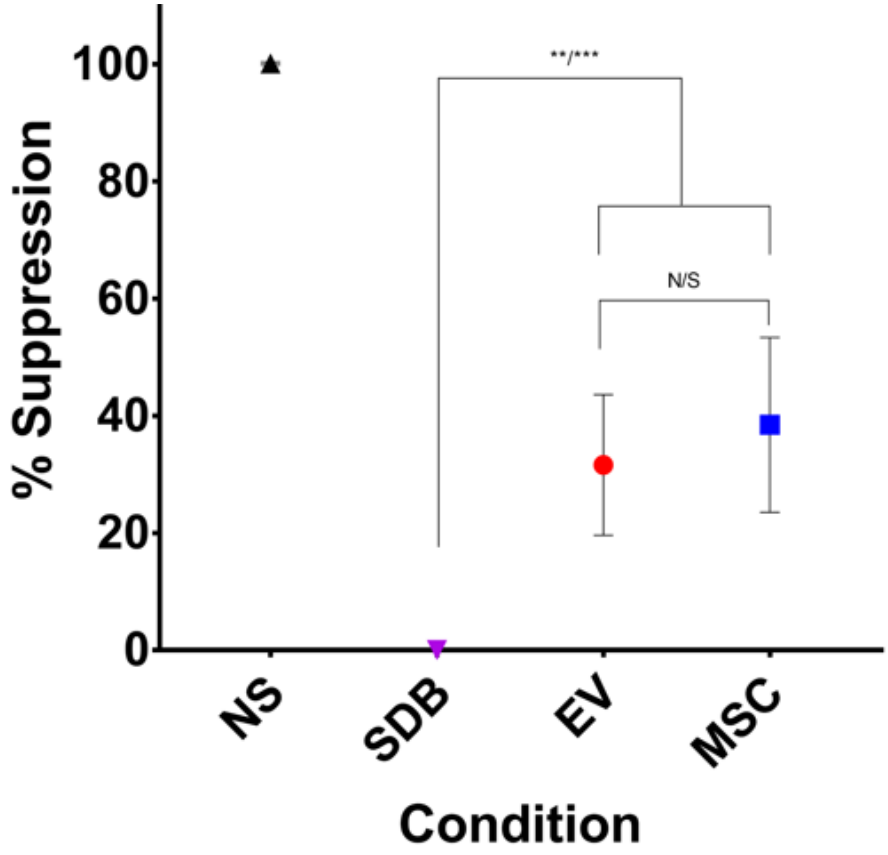


**Figure 20: hBM-MSCs/sEV potency for immune suppression confirmed by inhibition of activated PBMCs.** hBM MSCs or sEV from ECM derived from hBM-MSC-48RB/81RB/55RB/85RB were isolated using the TFF+FPLC workflow to address differences in MSCs and sEV potency at a set dose for immunomodulation of the PBMCs. Each hBM-MSC/MSC-EV donor was tested at either 0.3 MSCs per 1PBMC or 5000 particles per 1 PBMC. Results were obtained by CFSE proliferation dye assessment on the FACSAria (BD Bioscience) using the FACSDiva software, and the gating strategy was analyzed on FlowJo (Version 10). Percent suppression was calculated using min-max normalization of CFSE expansion index (EI) for each sample compared to the non-stimulated (min) and stimulated (max) controls. EV condition representative of all 4 hBM-MSC-sEV donor results combined. MSC condition

representative of all 4 hBM-MSCs donor results. NS representative of the non-stimulated PBMC control. SDB condition representative of activated PBMC control with CD3/28 dynabeads to determine proliferation rate following stimulation. N=3, independent experiments with 2 technical replicates. Analysis conducted on Graphpad Prism version 7, one way ANOVA with Tukey's multiple comparison test where; $p<0.05$ = *, $p < 0.01$ = **, $p <0.001$ = *** and $p < 0.0001$ = **** using one way ANOVA and Tukey post hoc analysis.

## Chapter 6: Discussion

Since the initial discovery of MSCs, increased investigation with new methodologies has expanded our understanding of what was initially considered a very minor cell population in the bone marrow to a highly relevant and functional subtype of "stem cell". With their inherent ability for immunomodulation and tissue repair, mesenchymal stromal cells have been at the foreground for cell-based therapeutic investigation. Furthermore, new insight into the mechanism of action has now shown us the significance of extracellular vesicles and their contribution to cellular signaling.

We began our investigation with the premise of improving upon the growing standards of MSC-based research and by association a better understanding of MSC-EV production and characterization. This was achieved by two specific components; the culture of MSCs in the hollow fiber cell bioreactor and secondly the high purity isolation of EVs for characterization. Prospective benefits of MSC culture in the bioreactor system are similar to those of 3D-based culture environments. Traditional 2D culture is drastically different from that of the *in-vivo* micro-environment and resultantly it has always been a concern that MSCs observed ex vivo are phenotypically and morphologically different from that of native MSCs. With a 3D system such as the hollow fiber bioreactor specifically, MSCs are returned to a multidimensional culture environment wherein they can behave more similar to that of their *in-vivo* counterpart by allowing for 3-dimensional branching of culture colonies while also allowing them a limited attachment to matrix structures. Additionally, 3D culture systems allow for dynamic changes in the cellular microenvironment such as oxygen tension and CO2 gas exchange. Furthermore and most importantly with 3D culture is the change in culture density. (82) Specifically in the bone marrow microenvironment, MSCs are not found evenly distributed in the local environment but usually

observed in the matrix layer between the endosteum and the vasculature of the bone marrow cross-section allowing from migration into the inner or out layer. (83) Compared to other 3D systems, the hollow fiber bioreactor culture system used in this study better emulates the matrix layer of bone marrow compared to spheroid or microcarrier-based bioreactor systems. (84, 85)

Foremost, under the guidelines of the ISCT (8), we validated our hBM-MSC cells obtained from RoosterBio Inc. for the minimal criteria confirming their expression of the MSC established surface proteins, their trilineage differentiation into osteocytes, chondrocytes, and adipocytes, and additionally their ability to adhere to plastic and matrix components. Furthermore, we were also able to show functional validation of the MSC's ability for immunomodulation improving upon the minimal criteria to display functional assessment. Even with the technological expansion of bioreactor systems for complex three-dimensional culture, very few studies have shown this form factor for EV production at this scale. Additionally, before our group, MSCs were not assessed for their ability to generate EVs for scalable long term bioreactor culture (25 days total), however, we were able to show that EVs have persistently produced from hBM-MSCs in the hollow fiber system for 25 days with minimal effect to the cells morphology or the EVs characteristics.

The MSCs were retrieved from the hollow fiber bioreactor for a full re-characterization as per the ISCT MSC minimal criteria to ensure persistent production for 25 days did not induce changes to the MSCs morphology or identity. We did note the temporal loss of CD105 expression and additionally the basal expression of CD34 (less than 10%) immediately following bioreactor harvest. When investigated, these changes were exhibited as transient and following returning the cells to their expansion media and 2D culture the cells returned to their originating state regaining full expression of CD105 and with no observed expression of the CD34. This transient expression of markers was observed in several other studies associated with bioreactor production and

additionally the use of serum-free media similar to the serum/xeno free cGMP compliant EV production media presented in this study. It is proposed this expression change is a result of adaptation to the aberrant bioreactor environment. (86, 87) Within the hollow fiber bioreactor, cells no longer attach in a planar fashion, with the ability to form complex 3D microstructures with neighboring cells, similar to that of the bone marrow microenvironment. It was observed that depending on the culture conditions and the attachment material, CD105 (Endoglin) expression will change as a surface attachment protein. (87) Additionally, representation of CD34 as negative identify criteria has recently come into question with several other groups reporting CD34+ expression of BM-MSC isolated from fresh bone marrow while retaining their MSC and stem-like qualities. (86, 88)

Additionally, we proceeded with a high purity method of isolation for the MSC-EVs with the combinational use of serum/xeno free production media and isolation by tangential flow filtration with bind-elute size exclusion chromatography and obtained a highly purified sample to improve the quality of our EV characterization. EVs produced under serum/xeno free condition and isolated by several methods to confirm the hBM-MSC-EV identity throughout the entire long-term production timeline as well as evaluate the functional ability of the EVs for therapeutic applications. Initially, EVs were isolated by PEG-based precipitation of the hBM-MSC ECM to assess the differences between EV production time points on a small scale (Less than 20mL of ECM). The results of this comparison confirmed that the EVs maintained their surface molecular profile and expression of EV associated proteins following the ISEV 2018 minimal information for characterization of EVs.(63) By protein classification of all 5 Categories we were able to show the particles isolated at each production time point were EVs from the MVB molecular pathway. Additionally, nanoparticle tracking analysis was completed to characterize the particles based on

the overall size as well as size distribution. When comparing hBM-MSC-EVs from each time point by NTA it was confirmed the EVs observed were less than 200nm in diameter for their average population as well as their population distribution confirm they are "small EVs" as per the ISEV guidelines. (63)

High purity scalable isolation was an essential criterion to evaluate with the bioreactor production of EVs from hBM-MSCs to validate their characterization done by PEG-based analysis as well as obtained a highly purified EV sample for functional assessment of immunomodulation. Following confirmation that the EVs isolated from all time points of hBM-MSC-EV production were of EV origin, time point samples from each donor were pooled and isolated in a large scale (greater than 100mL of ECM) multimodal ultrafiltration workflow to confirm a scalable high purity isolation method would improve EV characterization, validation of functionality and successfully achieve EV isolation that could be used for clinical investigation. The currently identified dynamic range of EV doses used for therapeutic applications ranged from particle concentrations from $10^6$ to $10^{10}$ particles per dose. Following tangential flow filtration and multimodal purification (Size exclusion and high-affinity protein binding) by FPLC particles were isolated in the sEV range (Less than 200nm) with a particle concentration at $10^9$ particles per mL which surpasses the required clinical investigation for most reported clinical trials including hBM-MSC-EVs used for graft-vs-host disease which showed a dose range at the top of the observed range with $1.35X\ 10^{10}$ particles total per dose. EVs from each donor was re-characterized following the full ISEV recommendations using the high purity isolation method and re-affirmed the EV identity with the presentation of EV-associated markers. With the combined scalable production of EVs with a scalable ultrafiltration isolation method, preclinical highly purified EVs dosing schemes could be achieved without strenuous production.

Furthermore, functional determination of hBM-MSC and hBM-MSC-EVs for immunomodulation was evaluated by their ability to suppress TCR activated PBMCs similar to the inflammatory response of GvHD and sepsis as an in-vitro assessment of their functionality. Dosing analysis was completed to identify the sensitivity of stimulated PBMCs to hBM-MSC-EVs ranging from 2500 particles per cell to 12500 particles per cell. The suppressive response of PBMCs to EVs at the lowest range of 2500 particles per cell showed 25% suppressive activity and with incremental increases in particle concentration, the increased suppressive activity was marginal with the highest dose showing statistically significantly ($p$-value $< 0.01$) results but at 5-times the concentration of the lowest dose. Independent of dosing, All MSC and EV conditions were able to significantly suppress the activated PBMCs ($p$-value$< 0.0001$) compared to stimulated control (SDB).

A key aspect of biologics-based therapies is the variability associated with individual donor material. Donor to donor variability has been an area of contention concerning cell-based therapies, demonstrating the limits of primary material for expansion and therapeutic potency between samples even within the same donor material. For this reason, functional assessment of therapeutic products is essential for clinical applications to present material best suited for disease attenuation. We compared the hBM-MSCs and hBM-MSC-EVs for 4 donors to determine how donor to donor variability compared between cells and EVs for therapeutic potency. Some EVs showed improved suppression potential of their originating cells and vice versa. At this level of sensitivity is not certain if this relationship is independent of the donor as of yet, however, it is conclusive that regardless of the donor, all the EV samples achieved a suppressive response on activated PBMCs greater than 30% suppression and some cases outperformed the hBM-MSCs for suppressive activity at a dose of 5000 particles per cell. Independent of the donor, all MSC and EV conditions

were able to significantly suppress the activated PBMCs (p-value<0.0001) compared to stimulated control (SDB). Additionally, comparing the effect of sEVs to MSCs globally, we observed no statistically significant difference in the potency at this scale and dose which demonstrated the EVs were just as effective at suppressing the active PBMCs as the MSCs. This result is a confirmation of the pre-clinical potential of EVs as an alternative biological product and also supports the role of EVs in MSC signaling.

Finally, it is still not certain what the distinct mechanism of action of EV uptake and suppression of immune cells. It was proposed by Campos-Mora et al, that NRP1 contributes to the suppression of T regulatory cells through EV-NRP1 transfer from dendritic cells. The accumulation of NRP1 in the T cells resulted in anti-proliferative signaling and downregulation of the immune response. (37) Concerning hBM-MSC-EV, we have previously shown the persistent expression of NRP1 on hBM-MSC-EVs, specifically, the identification of NRP1 on all represented donors and additionally, surface presentation of NRP1 across the entire isolated EV population. In this study, we reproduced these results with 5 additional distinct donors to confirm NRP1 as an MSC-EV identity marker. Further to this, following MSC-EV production in a "closer to in-vivo" culture system with the addition of a high purity means of isolation were able to distinctly characterize the MSC-EVs with a higher degree of certainty as well as validate their functionally to mimic MSC behavior as immunomodulators. With the scope of this study, we were not able to identify a detailed mechanistic approach as to how the MSC-EV exert their effects; however, we speculate that some of the immunomodulatory potential observed in this study could be contributed to the transfer of hBM-MSC-EV NRP1 upon uptake to the activated T cell population to induce anti-proliferative effects as observed in other immunomodulatory studies. The MSC-EVs isolated in this study were assessed for the presence of traditional MSC immunomodulatory effectors such

as interleukins and growth factors at varying abundance (data not shown) so we can speculate the EVs alone may also be able to deliver the complimentary paracrine activity as a vesicle bundle with multifaceted signaling effects.

Additional experiments such as particle tracking and uptake of the hBM-MSC-EVs during the activated PBMC could be done to determine which immune cells are affected by the presence of EVs. An anti-NRP1 antagonist or NRP1 knockdown of the hBM-MSCs producing the EVs could be done to validate the contribution of EV-NRP1 to the suppressive activity by removing or reduce its presentation to observe how the activated PBMCs respond. Furthermore, EV engineering of NRP1 constituents could also be done to further elucidate now much of the NRP1 signaling is functionally relevant. Additional characterization would also improve the resolution of the results obtained in this study such as single EV analysis to determine the proportionality and heterogeneity of the EV population to provide a more in-depth understanding of what portion of the particle population contributes to distinct signaling mechanisms. Finally, report-tagged EVs could be used in-vivo following MSC or MSC-EV transplant to observe their systemic delivery and behavior.

## Chapter 7: Conclusion

In conclusion, to address the gaps in the literature regarding the functional ability of MSC-EVs following isolation as well as to strengthen the characteristic validation of our novel NRP1 presenting MSC-EVs, we proposed our investigation which we showed *NRP1 was expressed on the surface of hBM-MSC-EVs capable of eliciting immunosuppression in activated PBMCs.* With this investigation, we focused on the main gaps in current MSC-EV research. Firstly, we assessed the hBM-MSCs in the non-stimulating bioreactor environment to confirm maintenance of MSC population where we showed consistent validation of the MSCs. Furthermore, we produced and characterized EVs retrieved from the hBM-MSCs in a serum-free 3D bioreactor where we showed highly pure EVs as per the MIISEV2018 guidelines. We specifically characterized the persistent expression of NRP1 bioreactor produced hBM-MSC-EVs as previously established by our group and demonstrated the functionality of bioreactor produced NRP1 expressing hBM-MSC-EV for immune suppression of active immune cells. Conclusively, we were able to validate the novel MSC-EV marker NRP1 on multiple bone marrow-derived cell donors and demonstrated the MSC-EVs functional abilities compared to MSCs alone.

Appendix:

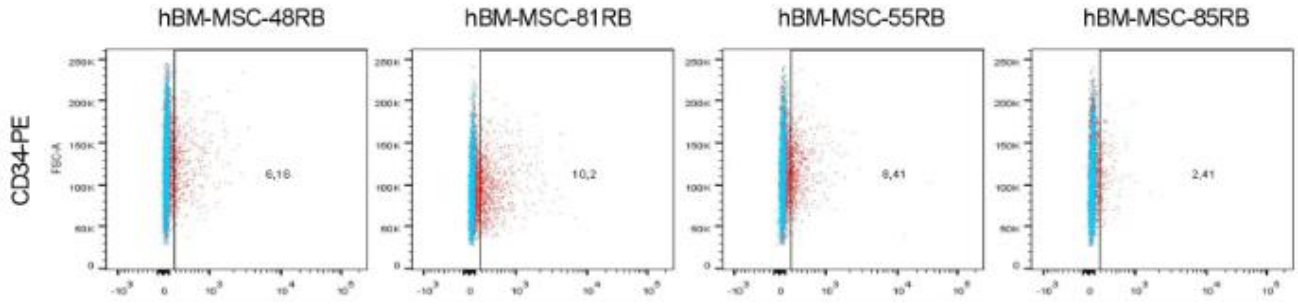


**Figure A1: hBM-MSC ISCT flow cytometry characterization of the negative marker expressed on the MSCs recovered post EV production was determined to be CD34.** Cytometric analysis of each negative marker present in the MSC negative marker antibody cocktail bioreactor-harvested from hBM-MSC-48RB/81RB/55RB/85RB identifying CD34 as staining marker. Red indicates the cell population stained with the respective antibodies. Blue indicates the cells stained with an IgG isotype control. Flow cytometry analysis was conducted on the BD Bioscience FACSAria Fusion, data collection was done using FACSDiva, and post-collection analysis was done using FlowJo Version 10.7. Samples were analyzed in duplicate with fluorophore compensation.

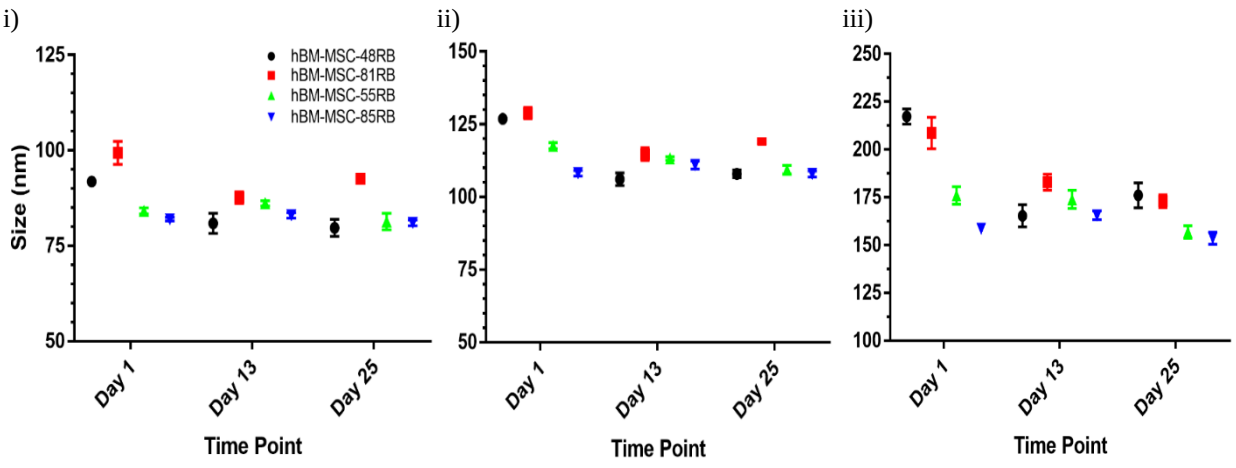

**Figure A2: Statistical Analysis of Nanoparticle Tracking Data Quantile Size Distribution of EVs isolated from hBM-MSC particle size range at different time points of production.** The percentile distribution of particle sizes for each hBM-MSC-EV sample from a different time point of Bioreactor EV production was observed following Nanoparticle Tracking Analysis to confirm the distribution of the observed particles determined by the ISEV 2018 guidelines. I) The 10$^{th}$ percentile of particles analyzed from each time point and donor, II) The 50$^{th}$ percentile of particles analyzed from each time point and donor. III) The 90$^{th}$ percentile of particles analyzed from each time point and donor. Analysis performed on NS300 using NTA3.0 software. Individual dots are representative of 5 technical replicates.

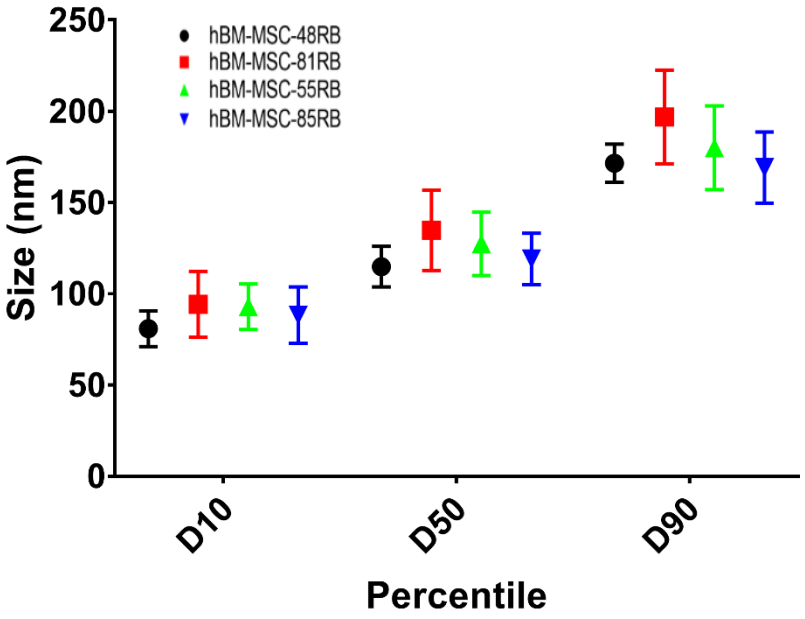


**Figure A3: Assessment of TFF+FPLC purified hBM-MSC-sEV particle size range by percentile distribution.** The percentile distribution of particle sizes for each purified donor sample hBM-MSC-sEV was observed following Nanoparticle Tracking Analysis to confirm the distribution of the observed particles falls below the 200nm size suggestion for small EVs as

determined by the ISEV 2018 guidelines. The $10^{th}$ percentile, $50^{th}$ percentile, and $90^{th}$ percentile of measured particles for each hBM-MSC-EV donor showed particles less than 200nm relative to the mean distribution. EVs were analyzed on the NS300 (Malvern) using NTA 3.0 Software. N=3

**References:**


1. Nancarrow-Lei R, Mafi P, Mafi R, Khan W. A Systemic Review of Adult Mesenchymal Stem Cell Sources and their Multilineage Differentiation Potential Relevant to Musculoskeletal Tissue Repair and Regeneration. Curr Stem Cell Res Ther. 2017;12(8):601-10.
2. Mafi R, Hindocha S, Mafi P, Griffin M, Khan WS. Sources of adult mesenchymal stem cells applicable for musculoskeletal applications - a systematic review of the literature. Open Orthop J. 2011;5 Suppl 2:242-8.
3. Witt R, Weigand A, Boos AM, Cai A, Dippold D, Boccaccini AR, et al. Mesenchymal stem cells and myoblast differentiation under HGF and IGF-1 stimulation for 3D skeletal muscle tissue engineering. BMC Cell Biol. 2017;18(1):15.
4. Friedenstein AJ, Petrakova KV, Kurolesova AI, Frolova GP. Heterotopic of bone marrow. Analysis of precursor cells for osteogenic and hematopoietic tissues. Transplantation. 1968;6(2):230-47.
5. Andrzejewska A, Lukomska B, Janowski M. Concise Review: Mesenchymal Stem Cells: From Roots to Boost. Stem Cells. 2019;37(7):855-64.
6. Caplan AI. Mesenchymal stem cells. J Orthop Res. 1991;9(5):641-50.
7. Caplan AI. Adult mesenchymal stem cells for tissue engineering versus regenerative medicine. J Cell Physiol. 2007;213(2):341-7.
8. Dominici M, Le Blanc K, Mueller I, Slaper-Cortenbach I, Marini F, Krause D, et al. Minimal criteria for defining multipotent mesenchymal stromal cells. The International Society for Cellular Therapy position statement. Cytotherapy. 2006;8(4):315-7.
9. Rodriguez-Fuentes DE, Fernandez-Garza LE, Samia-Meza JA, Barrera-Barrera SA, Caplan AI, Barrera-Saldana HA. Mesenchymal Stem Cells Current Clinical Applications: A Systematic Review. Arch Med Res. 2021;52(1):93-101.
10. Caplan AI. Mesenchymal Stem Cells: Time to Change the Name! Stem Cells Transl Med. 2017;6(6):1445-51.
11. Pacini S, Petrini M. Editorial: In Search of In vivo MSC. Front Cell Dev Biol. 2017;5:60.
12. da Silva Meirelles L, Caplan AI, Nardi NB. In search of the in vivo identity of mesenchymal stem cells. Stem Cells. 2008;26(9):2287-99.
13. Pittenger MF, Discher DE, Peault BM, Phinney DG, Hare JM, Caplan AI. Mesenchymal stem cell perspective: cell biology to clinical progress. NPJ Regen Med. 2019;4:22.
14. Cheng Y, Cao X, Qin L. Mesenchymal Stem Cell-Derived Extracellular Vesicles: A Novel Cell-Free Therapy for Sepsis. Front Immunol. 2020;11:647.
15. Hwang NS, Zhang C, Hwang YS, Varghese S. Mesenchymal stem cell differentiation and roles in regenerative medicine. Wiley Interdiscip Rev Syst Biol Med. 2009;1(1):97-106.
16. Mushahary D, Spittler A, Kasper C, Weber V, Charwat V. Isolation, cultivation, and characterization of human mesenchymal stem cells. Cytometry A. 2018;93(1):19-31.
17. Elahi KC, Klein G, Avci-Adali M, Sievert KD, MacNeil S, Aicher WK. Human Mesenchymal Stromal Cells from Different Sources Diverge in Their Expression of Cell Surface Proteins and Display Distinct Differentiation Patterns. Stem Cells Int. 2016;2016:5646384.
18. Hendijani F. Explant culture: An advantageous method for isolation of mesenchymal stem cells from human tissues. Cell Prolif. 2017;50(2).
19. Wu X, Jiang J, Gu Z, Zhang J, Chen Y, Liu X. Mesenchymal stromal cell therapies: immunomodulatory properties and clinical progress. Stem Cell Res Ther. 2020;11(1):345.

20. Leuning DG, Beijer NRM, du Fosse NA, Vermeulen S, Lievers E, van Kooten C, et al. The cytokine secretion profile of mesenchymal stromal cells is determined by surface structure of the microenvironment. Sci Rep. 2018;8(1):7716.
21. Ullah M, Liu DD, Thakor AS. Mesenchymal Stromal Cell Homing: Mechanisms and Strategies for Improvement. iScience. 2019;15:421-38.
22. Fu X, Liu G, Halim A, Ju Y, Luo Q, Song AG. Mesenchymal Stem Cell Migration and Tissue Repair. Cells. 2019;8(8).
23. Jiang D, Scharffetter-Kochanek K. Mesenchymal Stem Cells Adaptively Respond to Environmental Cues Thereby Improving Granulation Tissue Formation and Wound Healing. Front Cell Dev Biol. 2020;8:697.
24. Weiss ARR, Dahlke MH. Immunomodulation by Mesenchymal Stem Cells (MSCs): Mechanisms of Action of Living, Apoptotic, and Dead MSCs. Front Immunol. 2019;10:1191.
25. Melief SM, Geutskens SB, Fibbe WE, Roelofs H. Multipotent stromal cells skew monocytes towards an anti-inflammatory interleukin-10-producing phenotype by production of interleukin-6. Haematologica. 2013;98(6):888-95.
26. Negi N, Griffin MD. Effects of mesenchymal stromal cells on regulatory T cells: Current understanding and clinical relevance. Stem Cells. 2020;38(5):596-605.
27. Laing AG, Fanelli G, Ramirez-Valdez A, Lechler RI, Lombardi G, Sharpe PT. Mesenchymal stem cells inhibit T-cell function through conserved induction of cellular stress. PLoS One. 2019;14(3):e0213170.
28. Osborne BA, Minter LM. Notch signalling during peripheral T-cell activation and differentiation. Nat Rev Immunol. 2007;7(1):64-75.
29. Winston Y. Cheung OH, Jonathan M. Gobin, Gauri Muradia, Jelica Mehic, Carole Westwood, and Jessie R. Lavoie Efficient Nonviral Transfection of Human Bone Marrow Mesenchymal Stromal Cells Shown Using Placental Growth Factor Overexpression. Stem Cell International. 2018.
30. Gelijns AC. MSCs in COVID-19 ARDS: U.S National Library of Medicine; 2020 [Available from: https://clinicaltrials.gov/ct2/show/NCT04371393.
31. Hwang JJ, Rim YA, Nam Y, Ju JH. Recent Developments in Clinical Applications of Mesenchymal Stem Cells in the Treatment of Rheumatoid Arthritis and Osteoarthritis. Front Immunol. 2021;12:631291.
32. Rad F, Ghorbani M, Mohammadi Roushandeh A, Habibi Roudkenar M. Mesenchymal stem cell-based therapy for autoimmune diseases: emerging roles of extracellular vesicles. Mol Biol Rep. 2019;46(1):1533-49.
33. Lanzoni G, Linetsky E, Correa D, Messinger Cayetano S, Alvarez RA, Kouroupis D, et al. Umbilical cord mesenchymal stem cells for COVID-19 acute respiratory distress syndrome: A double-blind, phase 1/2a, randomized controlled trial. Stem Cells Transl Med. 2021;10(5):660-73.
34. Cooke KR, Luznik L, Sarantopoulos S, Hakim FT, Jagasia M, Fowler DH, et al. The Biology of Chronic Graft-versus-Host Disease: A Task Force Report from the National Institutes of Health Consensus Development Project on Criteria for Clinical Trials in Chronic Graft-versus-Host Disease. Biol Blood Marrow Transplant. 2017;23(2):211-34.
35. Massa M, Croce S, Campanelli R, Abba C, Lenta E, Valsecchi C, et al. Clinical Applications of Mesenchymal Stem/Stromal Cell Derived Extracellular Vesicles: Therapeutic Potential of an Acellular Product. Diagnostics (Basel). 2020;10(12).
36. Fujii S, Miura Y, Fujishiro A, Shindo T, Shimazu Y, Hirai H, et al. Graft-Versus-Host Disease Amelioration by Human Bone Marrow Mesenchymal Stromal/Stem Cell-Derived

Extracellular Vesicles Is Associated with Peripheral Preservation of Naive T Cell Populations. Stem Cells. 2018;36(3):434-45.
37. Campos-Mora M, Contreras-Kallens P, Galvez-Jiron F, Rojas M, Rojas C, Refisch A, et al. CD4+Foxp3+T Regulatory Cells Promote Transplantation Tolerance by Modulating Effector CD4+ T Cells in a Neuropilin-1-Dependent Manner. Front Immunol. 2019;10:882.
38. Podesta MA, Remuzzi G, Casiraghi F. Mesenchymal Stromal Cells for Transplant Tolerance. Front Immunol. 2019;10:1287.
39. Sun XY, Ding XF, Liang HY, Zhang XJ, Liu SH, Bing H, et al. Efficacy of mesenchymal stem cell therapy for sepsis: a meta-analysis of preclinical studies. Stem Cell Res Ther. 2020;11(1):214.
40. Lombardo E, van der Poll T, DelaRosa O, Dalemans W. Mesenchymal stem cells as a therapeutic tool to treat sepsis. World J Stem Cells. 2015;7(2):368-79.
41. Yang Y, Ye Y, Su X, He J, Bai W, He X. MSCs-Derived Exosomes and Neuroinflammation, Neurogenesis and Therapy of Traumatic Brain Injury. Front Cell Neurosci. 2017;11:55.
42. Wang XJ, Li QP. The roles of mesenchymal stem cells (MSCs) therapy in ischemic heart diseases. Biochem Biophys Res Commun. 2007;359(2):189-93.
43. Chelluboina B, Dinh DH, Veeravalli KK. Transdifferentiation of differentiated stem cells contributes to remyelination. Stem Cell Res Ther. 2015;6:191.
44. Ham O, Lee CY, Kim R, Lee J, Oh S, Lee MY, et al. Therapeutic Potential of Differentiated Mesenchymal Stem Cells for Treatment of Osteoarthritis. Int J Mol Sci. 2015;16(7):14961-78.
45. Saeed H, Ahsan M, Saleem Z, Iqtedar M, Islam M, Danish Z, et al. Mesenchymal stem cells (MSCs) as skeletal therapeutics - an update. J Biomed Sci. 2016;23:41.
46. Zha K, Sun Z, Yang Y, Chen M, Gao C, Fu L, et al. Recent Developed Strategies for Enhancing Chondrogenic Differentiation of MSC: Impact on MSC-Based Therapy for Cartilage Regeneration. Stem Cells Int. 2021;2021:8830834.
47. Sottile F, Aulicino F, Theka I, Cosma MP. Mesenchymal stem cells generate distinct functional hybrids in vitro via cell fusion or entosis. Sci Rep. 2016;6:36863.
48. Lemcke H, Gaebel R, Skorska A, Voronina N, Lux CA, Petters J, et al. Mechanisms of stem cell based cardiac repair-gap junctional signaling promotes the cardiac lineage specification of mesenchymal stem cells. Sci Rep. 2017;7(1):9755.
49. Urrutia DN, Caviedes P, Mardones R, Minguell JJ, Vega-Letter AM, Jofre CM. Comparative study of the neural differentiation capacity of mesenchymal stromal cells from different tissue sources: An approach for their use in neural regeneration therapies. PLoS One. 2019;14(3):e0213032.
50. Krabbe C, Zimmer J, Meyer M. Neural transdifferentiation of mesenchymal stem cells--a critical review. APMIS. 2005;113(11-12):831-44.
51. Ullah M, Stich S, Notter M, Eucker J, Sittinger M, Ringe J. Transdifferentiation of mesenchymal stem cells-derived adipogenic-differentiated cells into osteogenic- or chondrogenic-differentiated cells proceeds via dedifferentiation and have a correlation with cell cycle arresting and driving genes. Differentiation. 2013;85(3):78-90.
52. Anderson HC. Vesicles Associated with Calcification in the matrix of Epiphyseal Cartilage. The Journal of Cell Biology. 1968.
53. Dalton AJ. Microvesicles and vesicles of multivesicular bodies versus "virus-like" particles. J Natl Cancer Inst. 1975;54(5):1137-48.

54. R M Johnstone MA, J R Hammond, L Orr, C Turbide. Vesicle formation during reticulocyte maturation. Association of plasma membrane activities with released vesicles (exosomes). The Journal of Biological Chemistry. 1987.
55. Vidal M. Exosomes: Revisiting their role as "garbage bags". Traffic. 2019;20(11):815-28.
56. Abels ER, Breakefield XO. Introduction to Extracellular Vesicles: Biogenesis, RNA Cargo Selection, Content, Release, and Uptake. Cell Mol Neurobiol. 2016;36(3):301-12.
57. Lotvall J, Hill AF, Hochberg F, Buzas EI, Di Vizio D, Gardiner C, et al. Minimal experimental requirements for definition of extracellular vesicles and their functions: a position statement from the International Society for Extracellular Vesicles. J Extracell Vesicles. 2014;3:26913.
58. Tang TT, Lv LL, Lan HY, Liu BC. Extracellular Vesicles: Opportunities and Challenges for the Treatment of Renal Diseases. Front Physiol. 2019;10:226.
59. Munshi A, Mehic J, Creskey M, Gobin J, Gao J, Rigg E, et al. A comprehensive proteomics profiling identifies NRP1 as a novel identity marker of human bone marrow mesenchymal stromal cell-derived small extracellular vesicles. Stem Cell Res Ther. 2019;10(1):401.
60. Ragni E, Banfi F, Barilani M, Cherubini A, Parazzi V, Larghi P, et al. Extracellular Vesicle-Shuttled mRNA in Mesenchymal Stem Cell Communication. Stem Cells. 2017;35(4):1093-105.
61. Martin-Rufino JD, Espinosa-Lara N, Osugui L, Sanchez-Guijo F. Targeting the Immune System With Mesenchymal Stromal Cell-Derived Extracellular Vesicles: What Is the Cargo's Mechanism of Action? Front Bioeng Biotechnol. 2019;7:308.
62. Bang OY, Kim EH. Mesenchymal Stem Cell-Derived Extracellular Vesicle Therapy for Stroke: Challenges and Progress. Front Neurol. 2019;10:211.
63. Thery C, Witwer KW, Aikawa E, Alcaraz MJ, Anderson JD, Andriantsitohaina R, et al. Minimal information for studies of extracellular vesicles 2018 (MISEV2018): a position statement of the International Society for Extracellular Vesicles and update of the MISEV2014 guidelines. J Extracell Vesicles. 2018;7(1):1535750.
64. Konoshenko MY, Lekchnov EA, Vlassov AV, Laktionov PP. Isolation of Extracellular Vesicles: General Methodologies and Latest Trends. Biomed Res Int. 2018;2018:8545347.
65. le Maire M, Champeil P, Moller JV. Interaction of membrane proteins and lipids with solubilizing detergents. Biochim Biophys Acta. 2000;1508(1-2):86-111.
66. Rider MA, Hurwitz SN, Meckes DG, Jr. ExtraPEG: A Polyethylene Glycol-Based Method for Enrichment of Extracellular Vesicles. Sci Rep. 2016;6:23978.
67. Sidhom K, Obi PO, Saleem A. A Review of Exosomal Isolation Methods: Is Size Exclusion Chromatography the Best Option? Int J Mol Sci. 2020;21(18).
68. Doyle LM, Wang MZ. Overview of Extracellular Vesicles, Their Origin, Composition, Purpose, and Methods for Exosome Isolation and Analysis. Cells. 2019;8(7).
69. Brennan K, Martin K, FitzGerald SP, O'Sullivan J, Wu Y, Blanco A, et al. A comparison of methods for the isolation and separation of extracellular vesicles from protein and lipid particles in human serum. Sci Rep. 2020;10(1):1039.
70. Midekessa G, Godakumara K, Ord J, Viil J, Lattekivi F, Dissanayake K, et al. Zeta Potential of Extracellular Vesicles: Toward Understanding the Attributes that Determine Colloidal Stability. ACS Omega. 2020;5(27):16701-10.
71. Rosu-Myles M, She YM, Fair J, Muradia G, Mehic J, Menendez P, et al. Identification of a candidate proteomic signature to discriminate multipotent and non-multipotent stromal cells. PLoS One. 2012;7(6):e38954.

72. Takagi S, Tsuji T, Amagai T, Takamatsu T, Fujisawa H. Specific cell surface labels in the visual centers of Xenopus laevis tadpole identified using monoclonal antibodies. Dev Biol. 1987;122(1):90-100.
73. Kolodkin AL, Levengood DV, Rowe EG, Tai YT, Giger RJ, Ginty DD. Neuropilin is a semaphorin III receptor. Cell. 1997;90(4):753-62.
74. Kolodkin AL, Ginty DD. Steering clear of semaphorins: neuropilins sound the retreat. Neuron. 1997;19(6):1159-62.
75. Fujisawa H. From the discovery of neuropilin to the determination of its adhesion sites. Adv Exp Med Biol. 2002;515:1-12.
76. Roy S, Bag AK, Singh RK, Talmadge JE, Batra SK, Datta K. Multifaceted Role of Neuropilins in the Immune System: Potential Targets for Immunotherapy. Front Immunol. 2017;8:1228.
77. Battin C, De Sousa Linhares A, Paster W, Isenman DE, Wahrmann M, Leitner J, et al. Neuropilin-1 Acts as a Receptor for Complement Split Products. Front Immunol. 2019;10:2209.
78. Raimondi C. Neuropilin-1 enforces extracellular matrix signalling via ABL1 to promote angiogenesis. Biochem Soc Trans. 2014;42(5):1429-34.
79. Plein A, Fantin A, Ruhrberg C. Neuropilin regulation of angiogenesis, arteriogenesis, and vascular permeability. Microcirculation. 2014;21(4):315-23.
80. Eichmann A, Simons M. VEGF signaling inside vascular endothelial cells and beyond. Curr Opin Cell Biol. 2012;24(2):188-93.
81. Niland S, Eble JA. Neuropilins in the Context of Tumor Vasculature. Int J Mol Sci. 2019;20(3).
82. Brenner AK, Andersson Tvedt TH, Bruserud O. The Complexity of Targeting PI3K-Akt-mTOR Signalling in Human Acute Myeloid Leukaemia: The Importance of Leukemic Cell Heterogeneity, Neighbouring Mesenchymal Stem Cells and Immunocompetent Cells. Molecules. 2016;21(11).
83. Castillo AB, Jacobs CR. Mesenchymal stem cell mechanobiology. Curr Osteoporos Rep. 2010;8(2):98-104.
84. Storm MP, Sorrell I, Shipley R, Regan S, Luetchford KA, Sathish J, et al. Hollow Fiber Bioreactors for In Vivo-like Mammalian Tissue Culture. J Vis Exp. 2016(111).
85. Gloeckner H, Lemke HD. New miniaturized hollow-fiber bioreactor for in vivo like cell culture, cell expansion, and production of cell-derived products. Biotechnol Prog. 2001;17(5):828-31.
86. Braun J, Kurtz A, Barutcu N, Bodo J, Thiel A, Dong J. Concerted regulation of CD34 and CD105 accompanies mesenchymal stromal cell derivation from human adventitial stromal cell. Stem Cells Dev. 2013;22(5):815-27.
87. Wang D, Liu N, Xie Y, Song B, Kong S, Sun X. Different culture method changing CD105 expression in amniotic fluid MSCs without affecting differentiation ability or immune function. J Cell Mol Med. 2020;24(7):4212-22.
88. Bellagamba BC, Grudzinski PB, Ely PB, Nader PJH, Nardi NB, da Silva Meirelles L. Induction of Expression of CD271 and CD34 in Mesenchymal Stromal Cells Cultured as Spheroids. Stem Cells Int. 2018;2018:7357213.

89. Malkin, E.Z., Bratman, S.V. Bioactive DNA from extracellular vesicles and particles. *Cell Death Dis* **11,** 584 (2020).

90. Tang, Y., Zhang, P., Wang, Y., Wang, J., Su, M., Wang, Y., Zhou, L., Zhou, J., Xiong, W., Zeng, Z., Zhou, Y., Nie, S. and Liao, Q., 2020. The Biogenesis, Biology, and Clinical Significance of Exosomal PD-L1 in Cancer. *Frontiers in Immunology*, 11.

91. Roy, Sohini, et al. "Multifaceted Role of Neuropilins in the Immune System: Potential Targets for Immunotherapy." *Frontiers in Immunology*, vol. 8, 2017, https://doi.org/10.3389/fimmu.2017.01228.